minerals

MDPI

Article

Assessment of Easily Accessible Spectroscopic Techniques Coupled with Multivariate Analysis for the Qualitative Characterization and Differentiation of Earth Pigments of Various Provenance

Ioana Maria Cortea [1,*], Luminița Ghervase [1,*], Roxana Rădvan [1] and George Serițan [2]

[1] Department of Optoelectronic Methods and Techniques for Artwork Restoration and Conservation, National Institute of Research and Development for Optoelectronics-INOE 2000, 077125 Magurele, Romania; radvan@inoe.ro

[2] Department of Measurements, Electrical Devices and Static Converters, University Politehnica of Bucharest, 060042 Bucharest, Romania; george.seritan@upb.ro

* Correspondence: ioana.cortea@inoe.ro (I.M.C.); ghervase@inoe.ro (L.G.)

Abstract: Natural minerals and earths with coloring properties have been widely used as artistic pigments since prehistoric times. Despite being extensively studied, the complex chemistry of earth pigments is still unsatisfactory described with respect to their mineralogical and structural variability and origin. In this study, a large group of earth pigments from various geographical locations was investigated using easily accessible spectroscopic techniques and multivariate analysis with the aim to identify distinctive mineralogical and chemical characteristics of natural pigment sources. Portable X-ray fluorescence (p-XRF), Fourier transform infrared spectroscopy (FTIR) and fiberoptic Raman spectroscopy were used for the elemental, molecular and structural characterization of the investigated pigments. Diagnostic spectral features and chemical patterns (fingerprints) were identified and discussed with respect to their geological sources. Due to the occurrence of similar accompanying minerals, it was observed that the differentiation of red and yellow ochers is more challenging compared to green, brown and black pigments. However, for some of the investigated pigments, the presence of certain accessory minerals and/or of certain chemical patterns can have diagnostic value. Principal component analysis (PCA) of the FTIR and XRF data matrices showed promising results in terms of geological attribution, highlighting a promising tool for provenance research. The results of the study demonstrate the potential benefits of this rapid and nondestructive approach for the characterization and differentiation of earth pigments with similar hues coming from different geological sources.

Keywords: earth pigments; ochers; FTIR; Raman; XRF; material characterization; spectroscopy; multivariate data analysis; provenance

Citation: Cortea, I.M.; Ghervase, L.; Rădvan, R.; Serițan, G. Assessment of Easily Accessible Spectroscopic Techniques Coupled with Multivariate Analysis for the Qualitative Characterization and Differentiation of Earth Pigments of Various Provenance. *Minerals* **2022**, *12*, 755. https://doi.org/10.3390/min12060755

Academic Editors: Katarzyna Chruszcz-Lipska and Urszula Solecka

Received: 9 May 2022
Accepted: 13 June 2022
Published: 14 June 2022

1. Introduction

Natural earths (iron and manganese oxides and hydroxides) are an important class of mineral pigments extensively used since prehistoric times due to their abundance, high coloring capacity and stability [1–3]. Earth pigments are often identified as colorful remains in archeological contexts—being used by ancient civilizations for decorative, medicinal, religious or symbolic purposes [2,4]. Natural minerals and earths with coloring properties have been used as pigments as early as 300,000 B.P. [5], and are frequently found in paleolithic figurative representations [6]; Egyptian art; ancient Greek, Hellenistic and Roman wall paintings; sculpture and architecture [7]. Earth pigments of various hues appear in illuminated manuscripts from European and Asian sources and in codices from pre-Hispanic South American cultures [7]. Probably the most commonly used inorganic

pigments of Byzantine and post-Byzantine iconography, earth pigments are also standard components, to this day, of the color palettes of European-tradition easel paintings [2,7,8].

Earth pigments can be broadly classified into iron-rich ochers, wads (manganese-rich ochers), umbers, green earths, white earths (chalks, kaolinite and diatomite), blue earths (vivianite-rich) and black earths (coals and other solid hydrocarbons) [4]. Depending on the variation in iron and manganese oxide composition, other references [7] propose a slightly different classification (see Table 1). The classification of these pigments is also affected by the terminology used, the nomenclature of earth pigments being complex (including archaic and historical names from documentary sources) and inconsistent [2]. For example, for red and yellow ochers alone, the Colour Index lists more than twenty alternative names (common, historic and marketing names). The definition of earth pigments is also vague, as it can vary in terms of mineralogical content from a natural earth, rich in clay minerals, iron and manganese oxides, to a fine fraction of pure iron oxide extracted from ferruginous sands [6–11]. A wide variety of other minerals, and even organic compounds (humic and fulvic acids), can also be present within the composition of certain types of earths, such as in the case of humic earth/lignite-based pigments [7].

Table 1. The main groups of earth pigments and their principal characteristics [7].

Group	Alternative Names	Color	Main Coloring Components
Ochers	ocher, flesh ochers, variations given by the geographical location of the source (e.g., Bristol ocher)	varying from browns and reds though yellows	iron oxide- and hydroxide-rich earths
Siennas	terre de Sienne, terra di Siena, Siena-erde	yellow-brown	iron hydroxide-rich earths + minor amounts of manganese oxides (<5%)
Umbers	ombra, terre d'ombre, terra d'ombra, tierra de sombra	warm brown to greenish brown	iron oxides + manganese oxides (between 5 and 20%)
Wads	bog manganese, black wad, black earth, manganese ochers	dark brown to black	iron oxides + manganese oxides (c. 50%)
Green earths	terra verde, terre vert, green stone	green to bluish green	clay minerals, celadonite or glauconite
Humic earths	Cassel earth, Cologne earth, Vandyke brown	rich brown	low-grade coal deposits or lignites

Depending on the constituent chromophore phases, earth pigments will produce a wide range of colors—from purple and red in the anhydrous oxides, to yellow, orange and brown in the oxide hydroxides [2,12]. In most cases, red ochers are dominated by hematite, while yellow ochers contain goethite and/or jarosite group minerals [2,10–13]. Depending on the environment that led to their formation, other iron minerals, such as maghemite, magnetite, lepidocrocite and akaganeite, may also be present in ochers [2,10]. In addition to iron hydroxide (goethite) particles, umbers and siennas contain various amounts of manganese oxides and/or oxyhydroxides—primarily the minerals manganite and pyrolusite (up to 20% in umbers and under 5% in siennas). Wads, on the other hand, contain up to 50% manganese oxides, a mixture of pyrolusite, birnessite, todorokite and romanechite, along with hydrated iron oxides, generally classified as limonite. Green earths are green to blue-green pigments derived from the minerals celadonite and glauconite. Besides their green coloring agents, green earths contain other minerals such as iron oxides, cronstedite, quartz, feldspar, amphiboles and various clay minerals—montmorillonite, illite, kaolinite, saponite [4,7].

Generally associated with various types of accessory minerals, such as silicates (e.g., clays, quartzes, and feldspars), carbonates, sulfates and aluminum hydroxides, the chemistry

of earth pigments is complex and still unsatisfactory described with respect to their mineralogical and structural variability and origin [10,13]. The type, amount and composition of these accessory minerals are mainly related to the source of extraction and to the degree of processing that the raw materials have undergone [2,10]. The preparation of earth pigments varies from little (simple grinding) or none to complex procedures, such as: washing the earth to remove the accessory minerals or any hard impurities; heating treatment in order to obtain various hues (red ocher from yellow ocher, burnt umber); the addition of other earth pigments and/or mineral fillers to achieve a desired color [2,14]. Whereas color is related to the nature of the chromophore present, differences in color may also be due to different mineralogical and chemical compositions (e.g., the presence of carbonate minerals) and/or differences in particle size [15]. As indicated in other works [7,9], an earth pigment's composition and color, as well as other working properties, is specific to its geological source.

Given the fact that earth pigments are ubiquitous in archaeological contexts, as well as in works of art from ancient times up to the modern period, their precise characterization is of great importance for understanding the archeological and art historical record, such as: raw material selection and use, provenance (geological origin) and the technology of paint production. Important information, especially in terms of use, have been obtained via the numerous case studies performed over time on a large variety of artifacts: prehistoric rock art [6,15,16], ancient wall paintings [17–20], religious art [8,21,22], easel paintings [23–26] and so on. However, within these case studies, the analyses are often limited to the identification of the generic class of earth pigment used (e.g., red ocher), without any specific characterization of the mineralogical species present or of the geological sources. Studies connecting earth pigments' mineralogy and structural variability with their sources (mainly sources from North America), have also been published [9,27–34], but to a lesser extent.

In this paper, a large group of earth pigments, of various hues and from different geographical regions, was investigated by means of complementary spectroscopic techniques and principal component analysis. More exactly, portable X-ray fluorescence (p-XRF), Fourier transform infrared spectroscopy (FTIR) in attenuated total reflection (ATR) mode and fiber-optic Raman spectroscopy were used for the elemental, molecular and structural characterization of the investigated pigments. Furthermore, a multivariate statistical treatment of the FTIR and XRF datasets was tested in order to gain an in-depth understanding of the variance within the samples. Specific, principal component analysis (PCA) was used to identify and classify samples of similar color but different origin (provenance). Most of the pigments investigated in this study came from important geological centers of pigment extraction and production in Europe, well documented since antiquity [7]. Based on the fact that the color and composition of earth pigments are locally specific and geologically controlled, the aim of the study was to assess if the selected methodology can highlight the existence of unique mineralogical and chemical signatures that could be used to discriminate between pigments of similar color tones from different locations.

As it is well documented in the literature, the complex chemistry and the occurrence of multicomponent mixtures makes the analysis of earth pigments challenging, and thus, for a complete characterization, a multi-analytical approach is most often necessary [35,36]. Earth pigments have been intensively studied over time via a wide range of analytical techniques [8–44]. Among the full range of modern analytical instrumentation, X-ray diffraction (XRD) stands among the most common techniques used to identify and characterize these types of pigments, as it can provide, in most cases, reliable data about the various mineral phases that might be present within the analyzed samples [30,37,45–47]. However, there may be situations in which overlapping diffraction lines (between iron oxides and the various accessory minerals) or the poor crystallinity of the sample can hinder an exact identification of the existing phases [2]. Fourier transform infrared spectroscopy and Raman vibrational spectroscopy also stand amidst the most frequently used techniques for mineral characterization and differentiation [2,8,13,48,49]. Along with handheld XRF analysis [50], these techniques are probably the most commonly used analytical tools in conservation science, as they offer a series of ad-

vantages such as: relatively low-cost, non- or minimal-invasiveness and an immediate response in terms of results [51]. Chemometrics, such as PCA, applied to different spectroscopic data, is a powerful analytical tool, widely used in recent years for discrimination analysis, including the classification of pigments [52,53]. In this study, the potential application value of easily accessible spectroscopic techniques (handheld XRF, ATR-FTIR and fiber-optic Raman), combined with chemometrics, was evaluated for the characterization and differentiation of earth pigments (of geological and mineralogical diversity).

2. Materials and Methods

2.1. Pigments Investigated in This Study

A set of 31 natural earth pigments from various geographical regions was selected for this study (Table 2). All pigments were purchased from Kremer Pigmente GmbH & Co. KG. Investigated pigments cover a wide range of colors—from pale yellow to golden hues (10 samples), reddish brown-violet to deep red (8 samples), brilliant green to greenish gray hues (6 samples), deep browns to gray-black hues (7 samples). Selected pigment samples came from different sources, including important ancient centers of pigment extraction and production located in Spain, France, Germany, Italy or Cyprus. All the analytical investigations were performed on powder samples (fine particle fraction < 120 μm). For each sample, we collected several point analyses in order to check for inhomogeneities. FTIR and XRF analyses were performed on the full set of pigments, while Raman spectroscopy was carried out only on a limited number of pigments (for situations where it was necessary to confirm or refine the FTIR data).

Table 2. Pigments investigated in this study. Pigments, obtained from Kremer Pigmente, are denoted by PK, followed by the catalog number.

Sample ID	Pigment (Commercial Name)	Hue	Color Index	Provenance (Origin)
PK11273	Red ocher from Andalusia	light-red	PR 102	Andalusia, Spain
PK11272	Yellow ocher from Andalusia	deep yellow	PY 43	Andalusia, Spain
PK11276	Brown ocher from Andalusia	reddish brown	PR 102	Andalusia, Spain
PK11280	Black earth from Andalusia	warm black	—	Andalusia, Spain
PK11584	Spanish red ocher	orange-red	PR 102	Castile, Spain
PK11575	Burgundy red ocher	orange-red	PR 102	Burgundy, France
PK11573	Burgundy yellow ocher	warm yellow	PY 43	Burgundy, France
PK11362	Gray from Burgundy	warm gray	—	Burgundy, France
PK11100	Bavarian green earth	light green	PG 23	Bavaria, Germany
PK40280	Amberg yellow	deep yellow	PY 43	Bavaria, Germany
PK40503	Red bole	orange-red	PR 102	Germany
PK11530	Lusatian ocher	brown-gold	PY 43	Saxony, Germany
PK11540	Taunus ocher	light warm yellow	PY 43	Hesse region, Germany
PK41050	Cassel brown	deep brown	NB 8	Cologne, Germany
PK40490	Rosso Sartorius	deep red	PR 102	Sardinia, Italy
PK40220	Italian gold ocher light	light gold	PY 43	Venice, Italy
PK40400	Raw Sienna Italian	deep yellow	PY 43	Tuscany, Italy
PK40260	Satin ocher	gold-orang	PY 43	Monte Amiata, Italy
PK11620	Brown earth from Otranto	sanguine-rust brown	PBr 7	Otranto, Italy
PK11010	Verona green earth	warm green	PG 23	Monte Baldo, Italy
PK11550	Snaefellsjoekull Red	reddish brown-violet	—	Snaefellsjoekull, Iceland
PK11551	Heydalsvegur Yellow	brown-gold	—	Snaefellsjoekull, Iceland
PK11552	Brimisvellir Green	moss green	—	Snaefellsjoekull, Iceland
PK17400	Green earth from Cyprus	brilliant green	PG 23	Cyprus
PK17410	Bluish green earth from Cyprus	brilliant bluish green	PG 23	Cyprus
PK40610	Raw umber from Cyprus	light warm brown	PBr 8	Cyprus
PK40710	Burnt umber from Cyprus	reddish deep brown	PBr 8	Cyprus
PK116431	Red Moroccan ocher	warm orange-red	PR 102	Midelt, Morocco
PK40623	Caledonian brown	intense brown	PBr 8	Morocco
PK11110	Russian green earth	light green	PG 23	Russia
PK40195	Gold ocher from Poland	light gold	PY 43	Carpathian Mts., Poland

2.2. Fourier Transform Infrared Spectroscopy (FTIR)

The infrared spectra of the pigments were registered in attenuated total reflection (ATR) mode using a SpectrumTwo FTIR spectrometer (PerkinElmer, Waltham, MA, USA) equipped with a GladiATR accessory (monolithic diamond ATR crystal from Pike Technologies, Fitchburg, WI, USA). Spectra were collected in the 4000–380 cm^{-1} mid-infrared spectral region at 4 cm^{-1} resolution. A total of 128 scans were used for an optimal signal-to-noise ratio. Data processing was carried out in Essential FTIR Spectroscopy Software Toolbox version 3.50.169 (Operant LLC, Monona, WI, USA).

2.3. X-ray Fluorescence (XRF)

XRF measurements were performed on the 31 powdered pigment samples using a portable energy-dispersive instrument from Bruker-TRACER III-SD, provided with a Rh anode X-ray tube and a 10 mm^2 X-Flash Silicon Drift Detector (SDD) with an energy resolution of approximately 147 eV for the Mn Kα line at 200,000 cps. All samples were measured in the same experimental conditions: 0,5 g of powder were measured and placed directly onto Mylar film so as to simulate an infinite layer thickness, then exposed to X-rays for 60 s. All spectra were collected in triplicate. The detection mode was universal, optimized for the mid-energy range of the 0–40 keV domain, and experimental parameters were set at 40 kV tube voltage and 10.60 μA current intensity with no filtering of the incident beam in air atmosphere. The instrument's detection limit, defined as three times the standard deviation, was calculated for each element. Element identification was conducted in ARTAX software using standard Bayesian deconvolution. Data processing and plotting were carried out in Excel 2016 and OriginPro 2021.

2.4. Raman Spectroscopy

Raman spectra were recorded using a WP 785 ER Raman Spectrometer (Wasatch Photonics, Logan, UT, USA) equipped with a standard fiber-optic probe, providing a spatial resolution of 7 cm^{-1}. A near-infrared diode laser (785 nm) was employed as the excitation source. The laser spot size was ~170 μm, while the collection area was 1 mm diameter at an 11 mm working distance (lens to sample). Acquisition time was on the order of 5 s and the laser power on the order of a few mW on the samples. The Raman spectra were acquired on powder pigments without any sample pretreatment. Some of the investigated pigments could not be characterized because of the strong luminescence they exhibit when using the 785 nm excitation wavelength. All the spectra were acquired in the absence of room lights to avoid any interference. Data collection was carried out in ENLIGHTEN Raman spectroscopy software version 2.2.7 (Wasatch Photonics Inc, Logan, UT, USA), while data processing was carried out in OriginPro version 8.0891.

2.5. Multivariate Data Analysis

Principal component analysis was performed on FTIR and XRF data using The Unscrambler X (v. 10.5.1) from CAMO Software version 10.5.1. As shown in previous studies [29,35,54], earth pigments can be highly heterogeneous and difficult to differentiate without the use of multivariate statistics. PCA is a powerful data-mining technique that can be used for exploratory analysis, to reduce data dimensionality and extract more interpretable information about the system under investigation [55,56]. PCAs were performed on data matrices constructed using the FTIR spectra of pigments by selecting specific IR regions in accordance with the characteristic absorptions of the main chromophores present in the samples. Separately, PCA was performed on the XRF spectra by incorporating the net area counts of the Kα (for elements with $Z < 45$) or Lα (for elements with $Z > 45$) peaks of each detected element related to the samples, normalized to the Rayleigh scattering peak of rhodium, Rh Kα, for each element [57–59]. The XRF spectral data were organized in a 31 × 22 matrix, where each line represented a pigment and the columns represented the counts corresponding to specific elements.

3. Results

3.1. Molecular Analysis

3.1.1. Red Ochers

The FTIR spectra registered on the red ochers investigated in this study are shown in Figure 1. A total of eight red earths from seven different geological sources were analyzed (see Table 2 for more details). The presence of hematite (Fe_2O_3) was identified in all samples through the characteristic IR absorptions present in the low frequency region: intense bands at c. 530 and 464 cm^{-1} [13]. Within the different red pigments analyzed, it was observed that the position of the first band (associated with hematite) varies between 534 and 526 cm^{-1}, while the position of the second band varies between 466–456 cm^{-1}. As shown in previous studies [2,10], these bands can be shifted up to 30 cm^{-1} depending on the particle size and morphology. For most of the samples, both bands are shifted to lower wavenumbers compared to the band position registered for the most common morphology encountered in hematite, with the second band at c. 464 cm^{-1} being more intense. These data indicate that the hematite particles are platy or elongated [10], most likely due to fine grinding that the pigments have undergone. The shift toward lower wavenumbers in the hematite IR bands could also be due to an increase in Al− for Fe− substitution in the hematite structure [60]. The Fe/Al substitution in the hematite structure was sustained by the registered Raman data (Figure 2a,b), which highlighted a broadening of the 225–290 cm^{-1} doublet and some upshift in the 405 cm^{-1} and 605 cm^{-1} peaks [41]. Besides hematite, the FTIR spectra registered strong absorptions associated with the presence of accessory minerals, mainly clays from the kaolin group and quartz. The aluminosilicate kaolinite ($Al_2Si_2O_5(OH)_4$) was clearly identified in samples PK40490, PK40503 and PK11575 via the characteristic hydroxyl bands at approx. 3700 and 3620 cm^{-1}, respectively, and via the band at 1030 cm^{-1} (Si-O-Si), 1004 cm^{-1} (Si-O-Si), 938 and 911 cm^{-1} (Al-O-H bands).

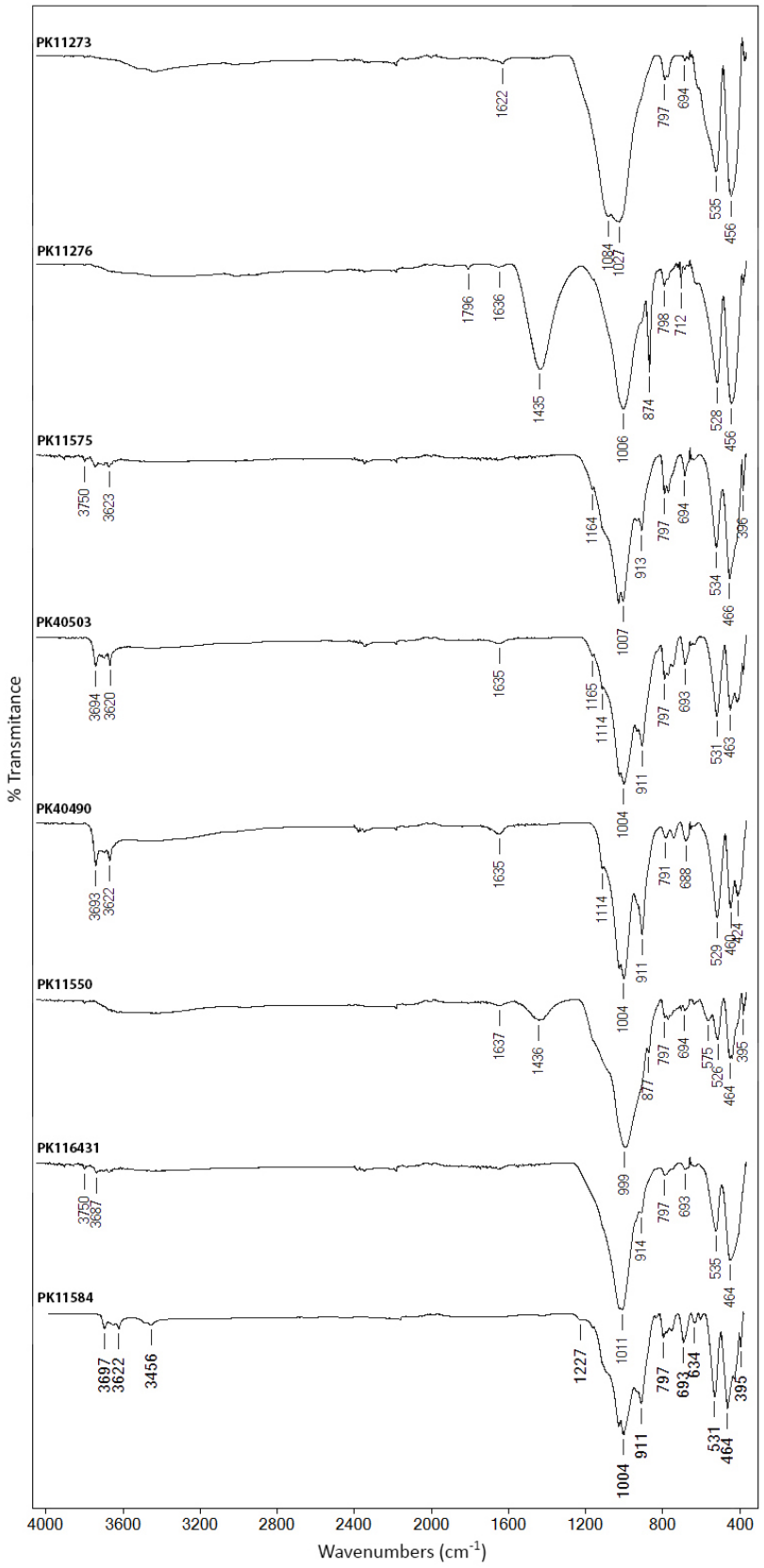

Figure 1. FTIR spectra registered on the red ochers.

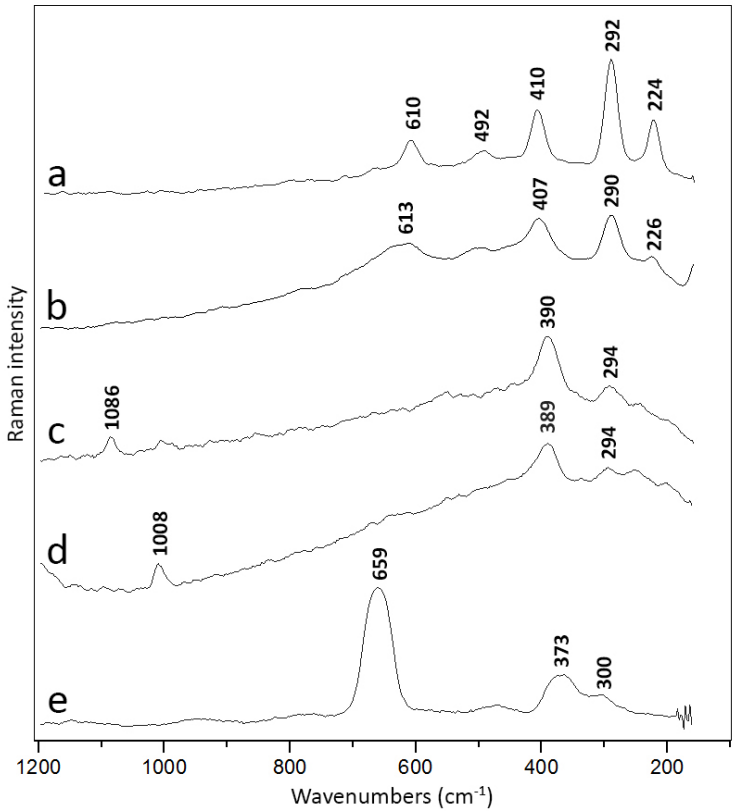

Figure 2. Raman spectra collected on: (**a**) sample PK11273; (**b**) sample PK40490; (**c**) sample PK40280; (**d**) sample PK40260; (**e**) sample PK40623.

Quartz (SiO_2) was also identified in varying amounts in all samples via the characteristic doublet observed at 797 and 778 cm^{-1} (Si–O symmetrical stretching vibration) and the peak at 694 cm^{-1} (Si–O symmetrical bending vibration) [13,61]. The main absorption in quartz, around 1080 cm^{-1} (Si–O antisymmetric stretching vibration), can be seen only in sample PK11273; within the other samples, this absorption was masked by the main Si-O-Si absorption of kaolinite. The presence of calcite ($CaCO_3$) was clearly highlighted in sample PK11276 via the fundamental vibrations of the carbonate ion in calcite—the broad absorption band centered at ~1435 cm^{-1} (ν_3 antisymmetric stretching), the two sharp bands at 872 (ν_2 out-of-plane bending) and 712 cm^{-1} (ν_4 in-plane bending) and the two small peaks at 2512 and 1795 cm^{-1} (combination bands) [62,63]. Small amounts of calcite can also be observed in sample PK11550.

A peak at 396 cm^{-1} can also be observed in most of the samples (except PK40490 and PK116431). Frequently found in ochers or earth-based pigments [18], this band is thought to be due to SiO_4–SiO_4 coupling in silicate [48], while other studies assign this band to Fe–O vibrations [64]. The shoulder band around 1165 cm^{-1}, observed in some of the spectra, can be linked to quartz. With the exception of sample PK11273, all other samples highlight within their spectra the presence of a small absorption around 1636(±1) cm^{-1}, ascribed to adsorbed water [60]. Within sample PK11273, the small but very characteristic peaks at 3480, 3401 and 1622 cm^{-1}, ascribed to stretching and deformation vibrations in the O–H bond, could be linked to the presence of low amounts of gypsum. However, with the exception of a small band at 673 cm^{-1} (S-O bend), no other characteristic absorption for sulfates can be seen; most probably, these small contributions are overlapped by the intense absorptions ascribed to quartz and hematite. Raman analysis confirmed the presence of low amounts of gypsum via the small but characteristic peaks observed at 1008 cm^{-1} and 492 cm^{-1} (Figure 2).

3.1.2. Yellow Ochers

Based on the FTIR spectra registered on the yellow pigments (Figure 3), two groups of ochers can be clearly distinguished: ochers rich in kaolinite and ochers rich in calcium sulfate (gypsum). Some of the analyzed yellow earth pigments fall outside both groups, being characterized by a different pattern (e.g., PK11530, PK11551). The characteristic IR absorptions for kaolinite (already mentioned in Section 3.1.1.) can be clearly observed in samples PK11573, PK11540, PK40400, PK40260 and PK40195 (Figure 3a). The presence of gypsum (hydrated calcium sulfate—$CaSO_4 \cdot 2H_2O$) is confirmed in samples PK40220 and PK40280 (Figure 3b) via the group of bands visible in the upper region of the spectra (3525, 3400 and 3240 cm^{-1}) and the bands at 1690 and 1620 cm^{-1}, ascribed to the O-H stretches and bends of the different water molecules present in gypsum. The characteristic vibrations of sulfate can be seen at 1100 cm^{-1} (S-O stretch) and around 668 and 597 cm^{-1} (S-O bends) [13]. The presence of quartz was clearly confirmed in some of the samples, a higher concentration being observed for the yellow ocher coming from Spain (PK11272). Calcium carbonate was also found, but to a lesser extent (samples PK40400 and PK40280); the presence of calcite was also confirmed with Raman via the characteristic peak at 1086 cm^{-1} [41].

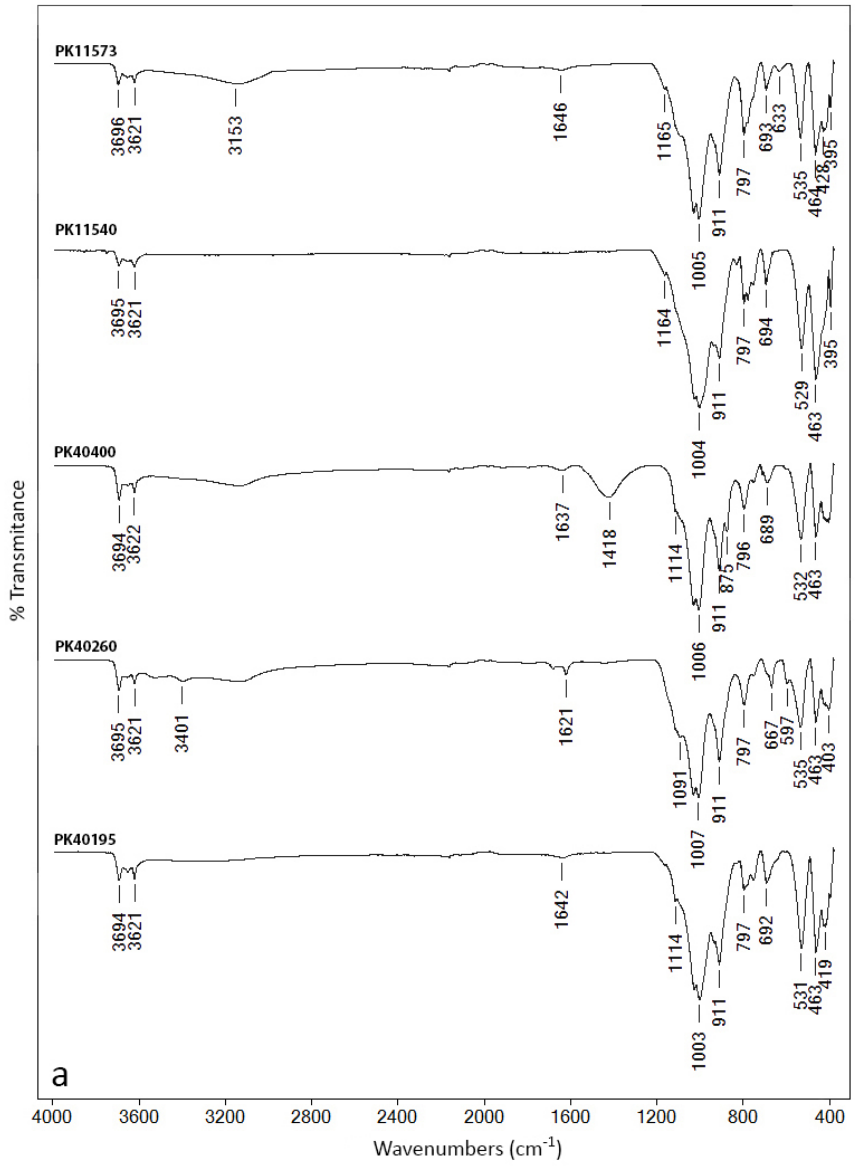

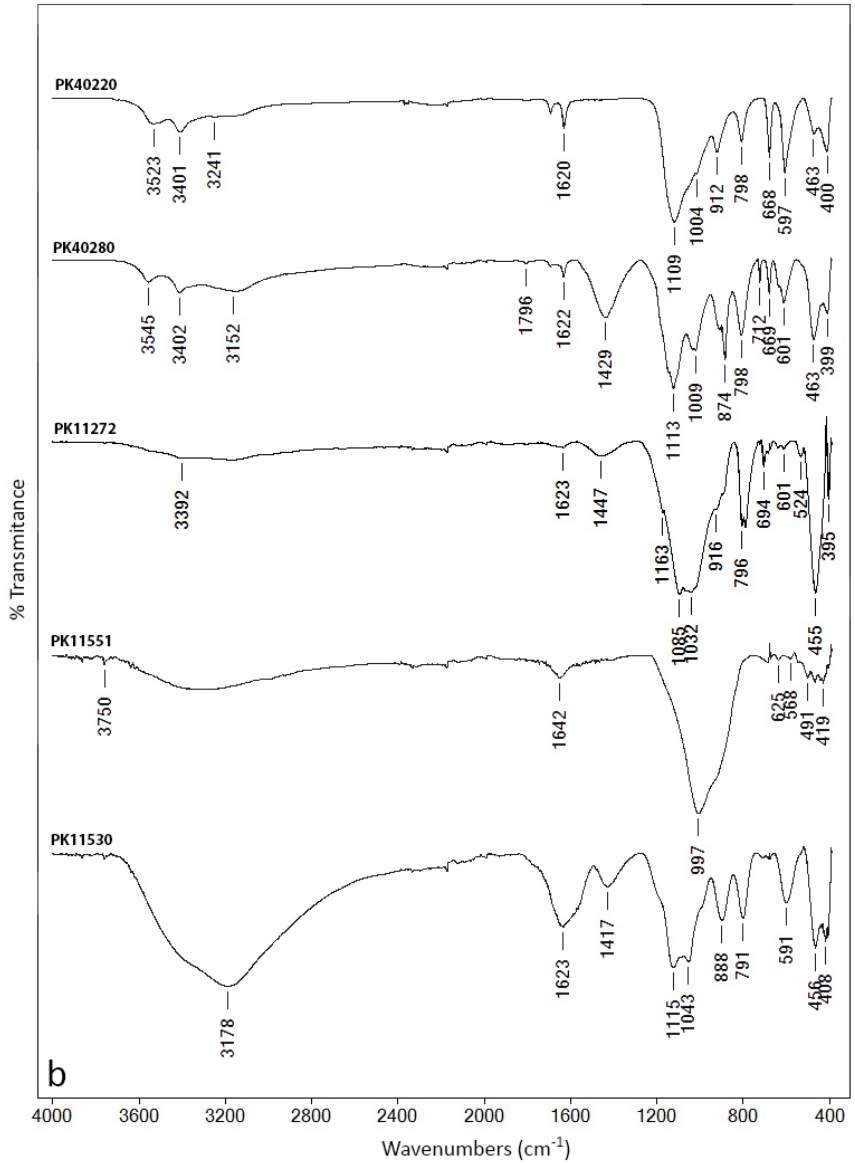

Figure 3. FTIR spectra registered on the yellow ochers: (**a**) ochers rich in kaolinite; (**b**) ochers rich in gypsum—samples PK40220 and PK40280.

Goethite (α-FeO(OH)), the main coloring agent in yellow-brown earths, could be clearly identified in some of the samples via the characteristic hydroxyl stretch at approximately 3150 cm^{-1} (broad, poorly defined band) and the hydroxyl deformation bands near 800 and 900 cm^{-1}. The lower energy bands in goethite are similar to those in hematite—sharp peaks at c. 530, 460 and 400 cm^{-1} ascribed to lattice vibrations [13,65]. For samples PK11272 and PK11573, a lattice band around 630 cm^{-1} can also be observed. As discussed in previous studies [10,65,66], several factors can affect the position of the goethite bands—including particle size, crystallinity, adsorbed water or the isomorphous substitution of iron by aluminum. The presence of silicates (especially quartz) and other clay minerals, even in low amounts, can also affect the identification of goethite, given the similar region of absorption [67]. Moreover, in situations when the hydroxyl stretch is partially obscured by the presence of water, a clear identification of goethite is less likely to be found using FTIR analysis alone. However, for such situations, the presence of goethite can be clearly confirmed with Raman analysis (Figure 2c,d) via the characteristic doublet observed at approx. 300 and 390 cm^{-1} [41].

The FTIR spectrum of sample PK11530 is dominated by: a broad OH stretching band in the 3400–3100 cm^{-1} range; the band at 1623 cm^{-1}, related to the O-H bending vibration in water; two peaks at 1115 and 1043 cm^{-1}. These two last peaks, along with the band at 591 cm^{-1}, can be ascribed to S-O stretches and bending vibrations in schwertmannite ($Fe_8O_8(OH)_6SO_4$), a hydroxysulfate mineral, commonly found in ocher deposits, formed from acid sulfate solutions [68,69]. The peaks around 888 and 791 cm^{-1} are specific to goethite.

Unlike most of the yellow ochers, which show a multitude of bands, the FTIR spectra of sample PK11551 are characterized by a simplified spectral signature with a dominant broad band at c. 1000 cm^{-1}. The overall pattern of the spectra indicates the presence of poor crystalline phases, as well as some possible overlapping contributions [70]. The weak bands at 3750 cm^{-1} and 1642 cm^{-1} correspond to O-H stretching and bending vibrations. Raman spectra registered on this pigment could not provide additional information due to the strong fluorescence background.

3.1.3. Green Earths

FTIR analysis of the green earth samples allowed for a clear distinction between samples containing celadonites and the ones containing glauconites. As can be easily observed in Figure 4, the samples from Cyprus (PK17400, PK17410) show characteristic absorptions for celadonite—sharp, narrow bands within the OH stretching region centered at 3603, 3580 (shoulder), 3558 and 3535 cm^{-1} [71,72]. Glauconites, on the other hand, are characterized by much broader absorptions within the OH stretching region, often poorly resolved, as in the case of sample PK11110, which exhibit a poorly defined peak at 3536 cm^{-1} and a shoulder band at 3604 cm^{-1}. As shown in previous studies [71], the OH bending vibration is situated at 800 cm^{-1} in celadonites, while samples containing glauconite (PK11110) exhibit a doublet—peaks at 800 and 815 cm^{-1}. The main absorption in celadonites is around 954 cm^{-1}, with a shoulder at 1072 cm^{-1} (Si-O stretching), while in glauconites, the main band is centered slightly higher—967 cm^{-1} in PK11110. Some small spectral variations within the low region of the spectra can also be observed and used to differentiate between the two green chromophores. In celadonite, the Si-O stretching and bending vibrations [72] are seen at 675, 490, 455 and 437 cm^{-1}, while in glauconite, these bands are slightly shifted to lower wavenumbers—672, 487, 451 and 431 cm^{-1}.

With the exception of the green earth pigment from Iceland (PK11552), all other green earth pigments display a small band around 1635 cm^{-1}, ascribed to hydroxyl bending [72]. The small band at 876 cm^{-1} (Al–Fe–OH vibration) observed in some of the samples (PK11100 and PK11010) could indicate a high Fe content in the octahedral sheet, possibly linked with the presence of Fe-smectite [31,73]. However, the same band, along with the small bump around 1430 cm^{-1}, is characteristic of calcium carbonate. For samples from Cyprus, the vibration at 840 cm^{-1} can be assigned to Al-Mg-OH vibrations. Compared to the rest of the group samples, pigments PK11100 and PK11552 contain high quartz content—peaks at 797, 779 and 693 cm^{-1}. For the same samples, the sharp band at 456 cm^{-1}, and the peak at 517 cm^{-1}—this last one observed only in PK11552—can be ascribed to Si–O bending vibrations [31].

The FTIR spectra registered on the green pigment from Iceland lack any characteristic absorptions for celadonite or glauconite. Instead, a broad spectral profile is observed in IR bands resolved at 1164, 1085 and 1056 cm^{-1}, which could be assigned to BO antisymmetric stretching vibrations in rhodizite ($(K,Cs)Al_4Be_4(B,Be)_{12}O_{28}$) [74], a pale green mineral frequently found on a matrix with quartz. The presence of rhodizite could not be confirmed via Raman analysis under the present experimental conditions (785 nm excitation wavelength) due to the significant fluorescence observed.

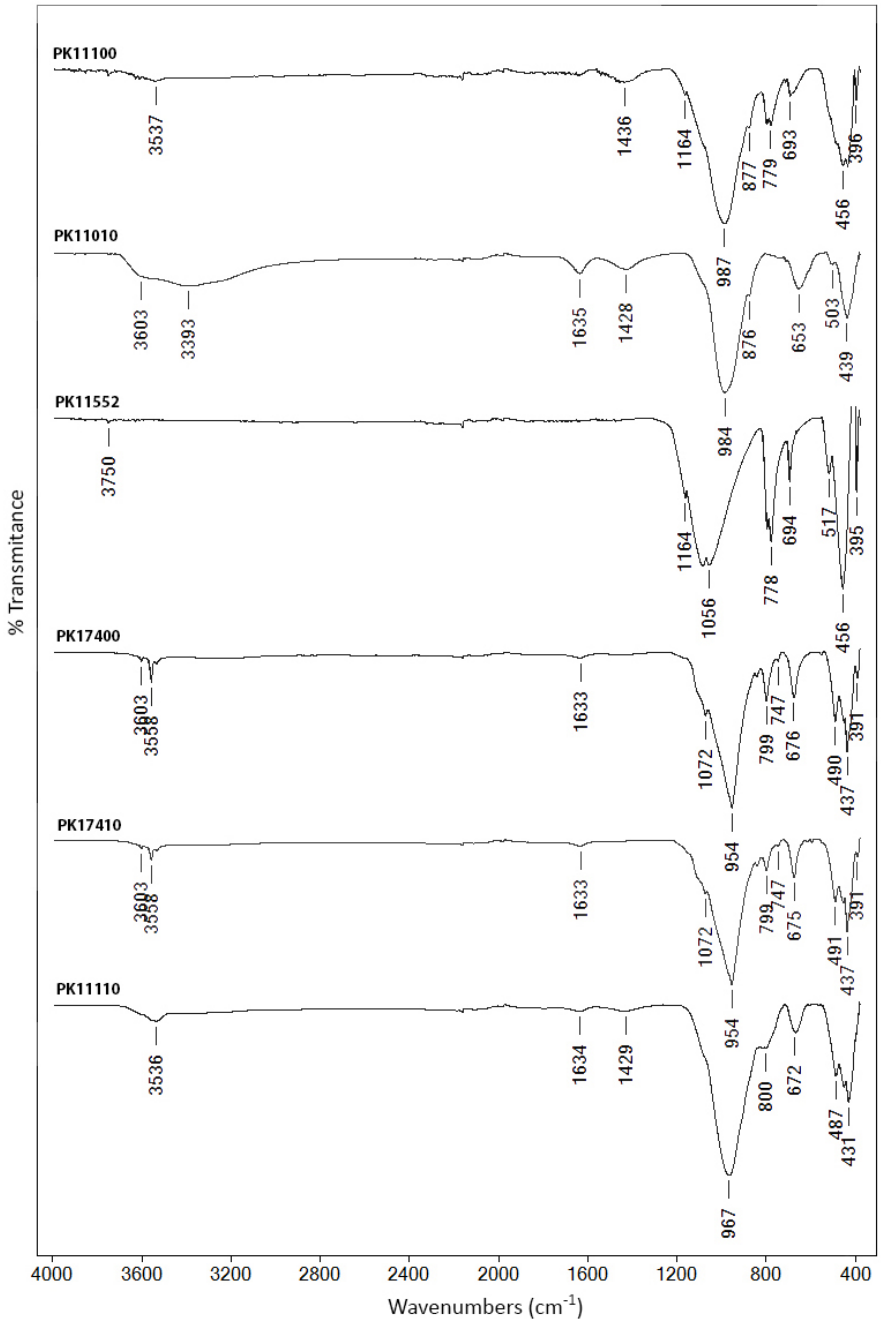

Figure 4. FTIR spectra registered on the green earth pigments.

3.1.4. Brown and Black Earths

Compared to the other group of analyzed pigments, the FTIR spectra registered on the brown and black earth pigments exhibit higher variation within their spectra (Figure 5). The FTIR spectrum registered on raw umber from Cyprus (sample PK40610) highlights the presence of goethite (characteristic peaks at 3190, 898 and 797 cm^{-1}), whereas within the burnt umber sample (PK40710), the presence of hematite was confirmed [13]. For umbers, manganese compounds should also be present in amounts between 5% to 20% [7].

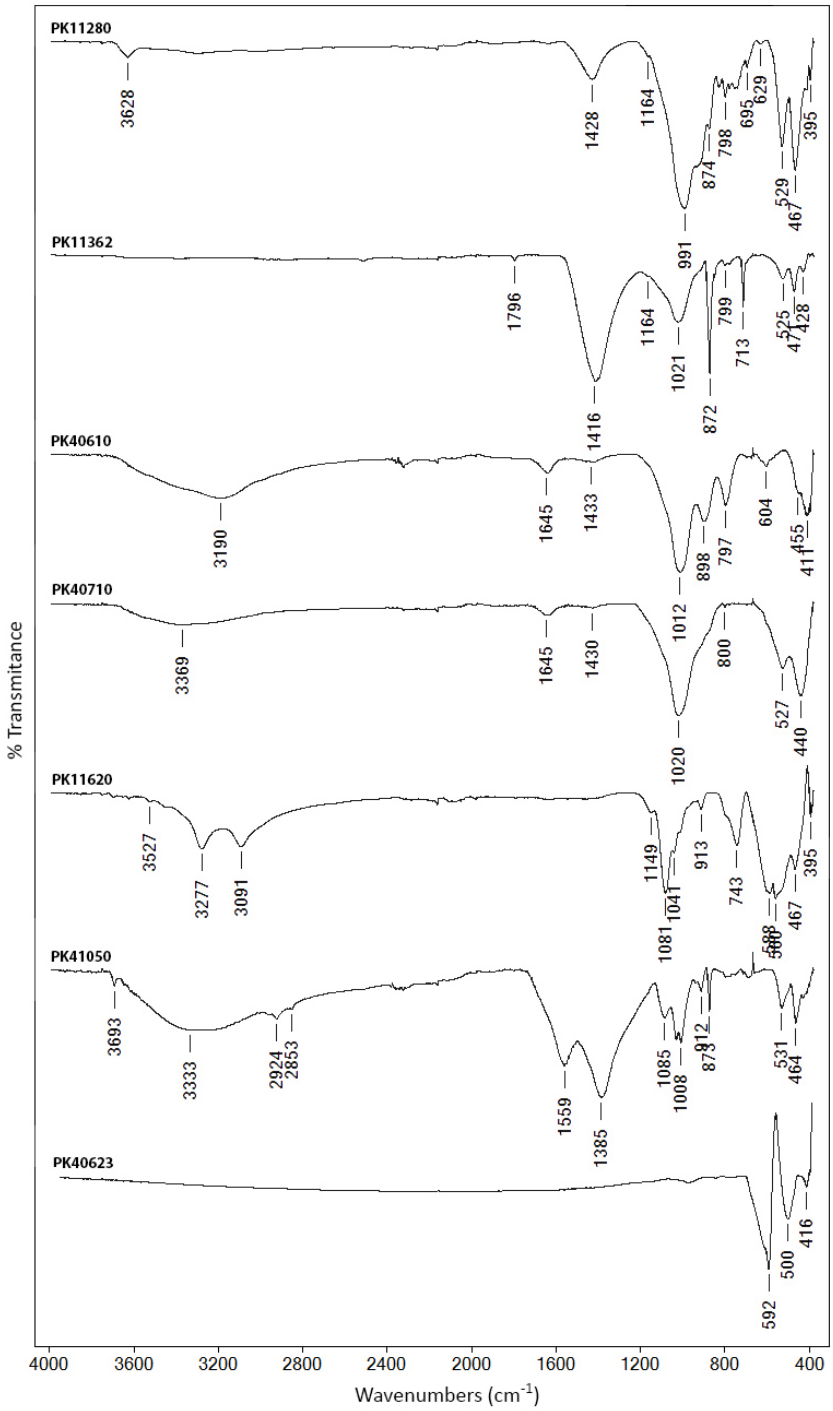

Figure 5. FTIR spectra registered on the brown and black earth pigments.

As show in previous studies, manganese dioxide (MnO_2), typically found in such pigments, should display a characteristic absorption around 1030 cm^{-1} [8,13]. In the analyzed samples from Cyprus, the main absorption is centered at 1012 cm^{-1} in raw umber and at 1020 cm^{-1} in burnt umber. This shift to lower wavenumbers could to be due to spectral interferences from other compounds that absorb in the same region, such as phyllosilicates [70]. Previous studies have found that Cyprus umbers contain palygorskite, a naturally occurring silicate mineral [75]. Raman analysis performed on these samples could not confirm the presence of

palygorskite, the registered spectra being characterized by weak, poorly resolved bands within the characteristic 400–1200 cm^{-1} region [76]. For these same samples, small amounts of calcite may also be present, as indicated by the small bump at 1430 cm^{-1}, while the vibration around 1645 cm^{-1} can be assigned to OH bending in bound water.

The gray earth from Burgundy (PK11362) displays a rich calcite content (intense peaks at 1416, 872, 713 cm^{-1}), along with small amounts of iron oxides and quartz. The black earth from Andalusia (PK11280) is characterized by the presence of iron oxides (intense peaks in the lower region of the spectra—529, 467 cm^{-1}), quartz, calcite and some clay minerals—possible chlorites, as indicated by the broad band at 3628 cm^{-1} (OH stretching) and the strong absorption around 991 cm^{-1} (Si-O stretching) [70]. Sample PK11620 (brown earth from Otranto) is characterized by two broad peaks in the upper region of the spectra (peaks at c. 3280 and 3090 cm^{-1}), which could indicate the presence of boehmite, an aluminum oxide hydroxide (γ-AlO(OH)) mineral [77], and by two intense bands, poorly defined, in the lower region of the spectra centered at c. 590 and 560 cm^{-1}, which may be ascribed to phosphate groups [78]. The peak around 1080 cm^{-1} is due to Si-O stretching in silicates, while the absorption band near 740 cm^{-1} is most probably associated with vibrations in the Si-O-Al bonds [70]. Iron oxides and small amounts of kaolinite are also present. FTIR spectra of Van Dyck Brown (sample PK41050) highlight the presence of humic substances (responsible for the dark color) together with a mineral fraction composed of clays and oxides. Typical bands for humic materials, the main components of organic matter in soils, seen at 3333, 1559 and 1385 cm^{-1}, can be ascribed to the carboxylic, aromatic and phenolic groups. The bands at 2924 and 2853 cm^{-1} (C–H stretching of methylene and methyl groups) are indicative of the presence of aliphatic chains in the macromolecule structure [78]. The general pattern registered is similar to that of brown coal and lignite [79]. The characteristic absorptions for kaolinite (3693, 1030, 1008, 912 cm^{-1}), calcite (873 cm^{-1}) and iron oxides (531, 464 cm^{-1}) can also be clearly seen in the spectra. Compared to the other brown and black pigments, sample PK40623 displays the most simplified spectra, with only a few sharp peaks in the lower wavenumber region—592, 500 and 416 cm^{-1}, most probably associated with metal–oxygen stretching and bending vibrations [80]. Raman analysis performed on this sample (Figure 2e) highlighted the presence of hausmannite (a brown-black manganese oxide mineral) via the characteristic bands observed at 659 cm^{-1} (strong and sharp band) and the smaller peaks at 373 and 300 cm^{-1} [81].

3.2. Elemental Analysis

Several elements have been identified in the analyzed samples, as shown in Table 3, in which elements are listed according to their relative contribution to the overall spectrum as major (ma)—defined as the main elements identified—minor (mi)—defined as the peaks ten times lower than the major peaks—and trace (tr) elements—defined as all other identified elements that were above the detection limit. The table does not include elements that were identified in the spectra but were lower than the calculated detection limit (Na and Mg were not detected above the LOD for any of the analyzed samples). Iron appears as the main element in the majority of samples, accompanied by Ca, K, Ti and Mn in minor or trace amounts, and several accessory elements, such as Al, Si, Zn, Nb, Y and Rb. Many of these minor/trace elements can be related either to the clay minerals or to the ferric oxides [82]. Some examples of XRF spectra are provided in Figure 6 for the red, brown, green and yellow pigments. Although they appear very similar, there are small differences between some of them. For instance, all three red pigments shown in Figure 6a have Fe as the main constituent, but the pigment from Sardinia, Italy (PK40490), has small traces of Ti, which are not seen in the other two pigments, while the red from Iceland has higher amounts of Ca, and the red pigment from Andalusia, Spain differentiates itself through its Zn and Pb content.

Table 3. Results of the XRF analysis.

Sample ID	Detected Elements
PK11273	Fe (ma), Zn (mi), Pb, Ca, Mn, K, Ti, As, Cu, Sr, Cr, S, Zr, Si, Ga (tr)
PK11272	Fe (ma), Ca, Pb, As, Cu, Ti, Cr, K, Zn, Si, S, Sr, Zr, Rb, Se, Ga (tr)
PK11276	Fe (ma), Ca (mi), Mn, K, As, Ti, Zn, Sr, Cu, Zr, Si, S, Ga (tr)
PK11280	Fe (ma), Ca, Mn, K, Ti (mi), Rb, Zr, Zn, Cr, Sr, Cu, Pb, Si, Ga, S, As (tr)
PK11584	Fe (ma), Ti, K, Mn, Sr, Ca, Zr, Rb, Cr, Cu, Zn, Si, Pb, S, Ga, Nb (tr)
PK11575	Fe (ma), Ti, K, Zr, Zn, Cr, Ca, Si, Cu, As, Y, Ga, Nb, Ge, S (tr)
PK11573	Fe (ma), Ti, K, Zr, Zn, Cr, Sr, Cl, Cu, Ca, As, Si, Ga, Y, S (tr)
PK11362	Ca (ma), Fe (mi), K, Sr, Ti, Mn, Rb, Cu, Si, S, Cr, S, Ga, Zn (tr)
PK11100	Fe (ma), Ca, K, Mn, Ti, Rb, Sr, Zr, Cr, Si, Cu, Pb, Zn, Ga (tr)
PK40280	Fe (ma), Ca (mi), Cu, Mn, Zn, S, Sr, Ti, V, As, K, Se, Ga, Si, Al (tr)
PK40503	Fe (ma), Ti, K, Zr, Rb, Zn, Ca, Y, Cr, Sr, Cu, Si, As, Ga, S (tr)
PK11530	Fe (ma), Ca, S, Ti, Cu, Cr, Ga, Y (tr)
PK11540	Fe (ma), K, Ti, Zr, Rb, Mn, Cr, Si, Cu, Sr, Zn, As, Ca, Ga, Nb, S (tr)
PK41050	Fe (ma), Ca, K, Ti (mi), Cu, Sr, As, Cr, Zr, Zn, S, Ga, Rb, Si, Nb, Al (tr)
PK40490	Fe (ma), Ti (mi), Mn, Ca, Rb, Sr, Zr, Cr, Cu, Nb, K, Si, Zn, Ga, S, Y (tr)
PK40220	Fe (ma), Ca (mi), Sr, S, Ti, Mn, K, Cu, Cr, Si, Zn, Ga (tr)
PK40400	Fe (ma), Ca, Ti (mi), Mn, Sr, Zr, Cr, Cu, As, Zn, Nb, K, Si, Ga, Y, S (tr)
PK40260	Fe (ma), Ca, Ti (mi), Mn, Sr, S, Zr, Cr, Cu, As, Zn, K, Nb, Si, Al (tr)
PK11620	Fe (ma), Ti (mi), Mn, Cr, Ca, Zr, Zn, Pb, Cu, Ga, Nb, Y, Al, Si (tr)
PK11010	Fe (ma), Ca, Ti (mi), Mn, Sr, K, Zr, Cr, Cu, Zn, Si, Nb, Y, Ga, S (tr)
PK11550	Fe (ma), Ca (mi), Ti, Mn, Sr, K, Cu, Si, Zr, Cr, Zn, Ga, Y, Nb (tr)
PK11551	Fe (ma), Ca (mi), Ti, Mn, Sr, Cr, K, Cu, Zr, Si, Zn, Nb (tr)
PK11552	Fe (ma), Ca, Ti, Mn (mi), Cr, Sr, K, Cu, Si, Zr, Zn, Ga, Y, Nb, S, Al (tr)
PK17400	Fe (ma), Mn, K, Ca, Ti, Cu, Cr, Si, Au, Zn, Y, Pb, Zr, Al, S (tr)
PK17410	Fe (ma), K, Mn, Ca, Ti, Rb, Zn, Cr, Cu, Sr, Si, Ga, Zr, S (tr)
PK40610	Fe (ma), Mn (mi), Ca, Sr, Ti, V, As, Cu, K, Zn, Si, Al (tr)
PK40710	Fe (ma), Mn (mi), Ca, Sr, V, Ti, Cu, Pb, K, Zn, Y, Mo, Si, As (tr)
PK116431	Fe (ma), Ti, Mn, K, Ca, Ba, Sr, Zn, Cu, Zr, Cr, Y, As, Si, Ga, S (tr)
PK40623	Mn (ma), Fe (mi), Ti, Pb, As, Cu, Ca, Al, Zn (tr)
PK11110	Fe (ma), K, Ca, Mn, Ti, Rb, Cr, Si, Sr, Cu, Zr, Au, Ga, S, Al, Zn, As (tr)
PK40195	Fe (ma), Ti, K, Mn, Rb, Sr, Zr, Ca, Cr, Cu, Si, Zn, As, Ga, Al (tr)

The brown pigment spectra, illustrated in Figure 6b, indicate that, while the Moroccan pigment has a very high Mn content, the pigment from Cyprus also has manganese, and the Mn:Fe ratio is quite the opposite from that of the Moroccan pigment; furthermore, the pigment from Cologne, Germany has an increased K ratio as compared to the other elements. Even fewer differences can be found in the green pigments shown in Figure 6c: there is a slightly higher level of Ca and Ti with respect to the main element, Fe, for the Cyprus-sourced pigment; a higher K:Fe ratio for the Russian and Italian pigments and a higher Mn input for the Italian pigment. The differences between the three German yellow pigments (Figure 6d) are very small; the Bavarian sample has somewhat higher Cu and Ca content, while the pigment from the Hesse region has more K and Ti.

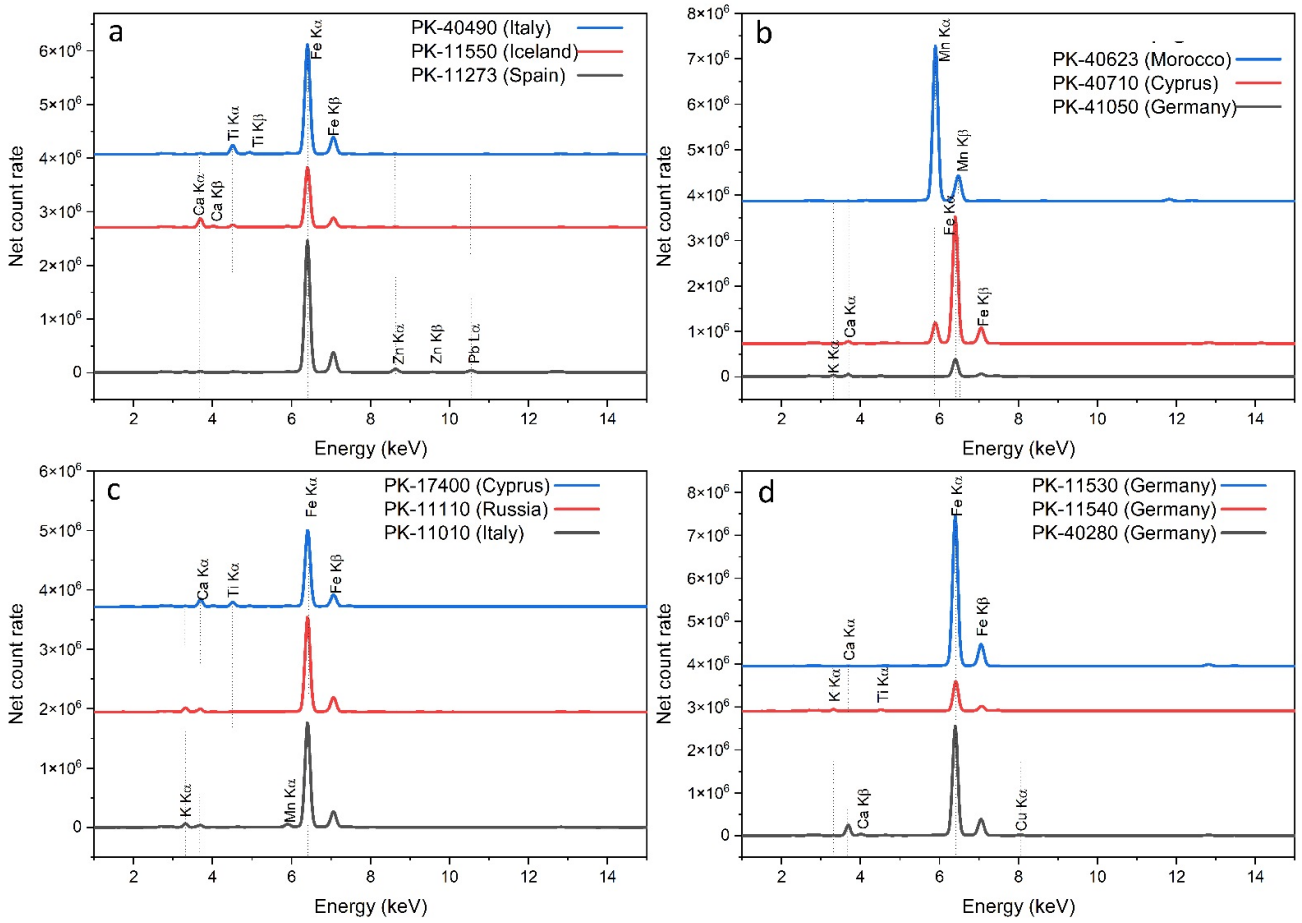

Figure 6. XRF spectra for some of the (**a**) red, (**b**) brown, (**c**) green and (**d**) yellow pigments.

Given their very similar composition, the distribution of the peak area associated with each element was plotted to achieve a better understanding of the relative contribution of each element as a function of their different sources (see Supplementary Materials). Peak areas were determined through a spectral deconvolution process, which takes into account theoretically calculated profiles.

While most pigments fall under the iron-rich ocher category, there were two exceptions: sample PK11362, the warm gray French pigment, which is very rich in calcium, and the sample from Morocco, the Caledonian brown (PK40623), which appears to belong to the wads category (manganese-rich ocher), and is also very high in copper. Potassium, which, in many cases, was found as a trace element, has the highest values in the green samples from Cyprus (PK17400, PK17410) and Russia (PK11110), of which, through FTIR analysis, the two Cyprus-originating pigments were identified as having celadonite, and the Russian pigment was identified as having glauconite—both potassium-rich minerals. Lead was found in all samples coming from Spain, and also in some of the brown pigments from Cyprus (PK40710), Italy (PK11620) and Morocco (PK40623). Strontium is part of many of the investigated pigments, but the highest levels were found for an Italian yellow (PK40220) and the two Cyprus-sourced brown pigments (PK40610, PK40710).

3.2.1. Red Ochers

The red ochers all show, relatively, medium iron levels, as compared to the other pigments. Some of them, especially from Italy and Iceland, show the presence of rare elements in trace amounts, such as Nb. The Spain-sourced red samples PK11584 and PK11273 have some Pb traces contrary to the other reds, which do not show any traces of lead; the latter sample

also has the greatest zinc content of all the investigated pigments. Rubidium is seen in only one red pigment, the one coming from Germany (PK40503). The Spanish reddish-brown sample, PK11276, and the red, PK11273, have higher As content, similar to another pigment from the same area, the yellow PK11272. One important thing to notice is that the red ocher pigment, PK116431, from Morocco, is the only one in the dataset that contains barium.

3.2.2. Yellow Ochers

The analyzed yellow pigments came from different sources located in six countries. Of them, Spain sample PK11272 shows the greatestPlease explain the color in the first column, or it should be removed according to our rules. As content of all the pigments, even though traces of this element are found in most of the analyzed samples. A noticeable amount of Cu is present in yellow sample PK40280, from Germany, and also in the Spanish yellow pigment, PK11272. Fe is present in all samples, in the majority of them as the main element; the one from Saxony, Germany (PK11530) has the highest content of Fe. Several yellows (PK40400, PK40260—Italy; PK11551—Iceland; PK11540—Germany) have a perceptible input from Nb. High rubidium concentrations were found for Germany-sourced sample PK11540 and for the yellow ochers from Poland (PK40195) and Spain (PK11272). Italian samples PK40220 and PK40260 have a greater S content as compared to the other pigments. Spanish sample PK40220 has the highest Sr input. Andalusian sample PK11272 shows the greatest lead input of all the pigments. Of all the detected elements, silica was found in almost every sample, with the greatest input in samples PK11272 (Spain) and PK11540 (Germany).

3.2.3. Green Earths

The green earth pigments showed slightly higher potassium levels, especially those from Cyprus (PK17400, PK17410) and Russia (PK11110). The PK17400 and PK11110 pigments additionally stand out through a higher aluminum content. Sample PK11552, from Iceland, appears to have more chromium than the rest of the green pigments. This pigment and the one from Russia both have more important contributions from Nb.

3.2.4. Brown and Black Earths

No general trend was highlighted for the black and brown pigments studied, but specific features stood out for some of the pigments. It can be pointed out that most of the brown pigments (except for PK41050) have no obvious Rb input. Italian sample PK11620 has the most significant chromium level in all the investigated samples, as well as high Zr and Nb content. Another sample that distinguishes itself from the rest is Moroccan PK40623, having the highest Mn content but the lowest iron contribution, which was the major element found for almost all other samples. The two samples from Cyprus, PK40710 and PK40610, also have very high input from manganese, as well as higher strontium. Moreover, these two pigments, along with German yellow PK40280, are the only ones in the entire dataset that have vanadium.

The black sample from Spain (PK11280) shows higher traces of some distinguishing elements, such as Zr, Rb and Nb. Contrary to the rest of the pigments, the major element found in the French black sample, PK11362, is Ca, not Fe, which is present only in minor amounts.

4. Discussion

4.1. Spectral and Chemical Fingerprints

4.1.1. Red Ochers

FTIR analysis indicated the presence of hematite in all the red ocher samples investigated, regardless of their provenance. The two sharp bands of hematite ascribed to Fe-O vibrations were observed at approx. 534–526 cm^{-1} and 466–456 cm^{-1}. For most of the investigated red earth pigments, the second band was more intense, inferring that the hematite particles are anisodimensional [2]. For unknown samples, the identification of hematite via FTIR analysis alone could be problematic, especially if certain accessory minerals are present in large amounts. Silicates or other clay minerals could mask the iron oxide

absorptions and prevent identification—quartz has two strong absorptions at 516 and 462 cm^{-1}, while kaolinite and illite display absorptions at approx. 540–530 cm^{-1} and 475 cm^{-1} [2]. Raman analysis can, however, confirm the presence of hematite and provide additional important information on Fe/Al substitution in the hematite structure.

In terms of IR spectral fingerprints, the red ochers from Burgundy (PK11575), Castile (PK11584) and Sardinia (PK40490), as well as the red bole from Germany (PK40503), are characterized by very similar spectra, with kaolinite as the main accessory mineral. Although the presence of kaolinite cannot be linked to a specific geological source, the hydroxyl bands intensities, as well as the band shape, can be used to differentiate certain pigments. Broader bands within the hydroxyl region suggest that the kaolin is relatively disordered, such as in the case of the red ochers coming from Burgundy and Castile, while sharper bands indicate well-crystalized kaolinite (samples from Sardinia and Germany) [10]. Various amounts of quartz were found in all samples investigated, but in significantly higher concentrations within the red ocher from Burgundy and the red bole from Germany. Compared to the rest of the analyzed samples, the red-brown ocher from Andalusia is characterized by a high calcium content.

XRF spectroscopy found several trace elements that could pertain to either the kandite, illite or smectite groups—Al, Si and K [83], almost ubiquitous in the red samples. While all samples mainly show the presence of the same chemical elements, the proportion between these elements varies from sample to sample. For instance, the red ochers from Spain, PK11584 (Castile) and PK11273 (Andalusia), show traces of lead, similar to another pigment from the same area, the deep-yellow PK11272. Similarly, PK11272, the Andalusian red, has a very high As content as compared to the other pigments, which seems likely to be a site-specific feature, as the other two Andalusian pigments (PK11272, PK11276) also have higher As levels compared to the rest of the dataset. From the point of view of its XRF composition, the reddish Iceland sample (PK11550) shows similar levels of Si, Zr, Ti and Sr compared to the other two samples from Iceland (the yellow PK11551 and the green PK11552). The red and green Iceland samples are characterized by the presence of rare elements, Nb and Y.

4.1.2. Yellow Ochers

The IR spectra of most of the yellow earth pigments investigated are dominated by absorptions due to accessory minerals. The yellow ochers from Burgundy (PK11573), the Hesse region (PK11540), Tuscany (PK40400, PK40260) and Poland (PK40195) are characterized by a rich kaolinite content, while the ones from Venice (PK40220) and Amberg (PK40280) are characterized by a rich gypsum content. The XRF analysis indicated that the Hesse region pigment has higher Nb and Rb, while the Poland sample has high Rb and Si. The Italian yellow pigments have low silica and high Sulphur content, with PK40220 having the greatest S input of all, as well as high Sr, and PK40280 having the highest Cu amount.

Goethite could be clearly identified via FTIR only when not masked by the presence of components with overlapping absorptions. Within the fingerprint region, the characteristic IR absorptions of goethite (bands at approx. 900 and 800 cm^{-1}) can me masked by the presence of kaolinite (absorption at 915 cm^{-1}) and quartz (doublet at 798 and 778 cm^{-1}), while in the upper region of the spectra, water adsorbed onto the surface of mineral particles gives rise to a broad absorption within 3400–3100 cm^{-1}, which can overlap the goethite hydroxyl stretch at approx. 3150 cm^{-1}. For such scenarios, Raman analysis can be used, as goethite is clearly detectable via the narrow doublet at 300 and 390 cm^{-1}, with no overlapping absorptions in this region.

The gold ocher from Saxony (PK11530) showed the most intense bands for goethite, with the hydroxyl stretch shifted to upper wavenumbers (3178 cm^{-1}), a sign for lower crystallinity content [2]. For the same sample, the FTIR spectrum highlighted the presence of schwertmannite, a poorly crystalline, metastable mineral that transforms spontaneously into goethite, frequently found in acid mine streams [84]. The yellow ocher from Andalusia (PK11272) is characterized by the highest quartz content, along some minor amounts of anhydrous calcium sulfate (anhydrite). For this same sample, XRF analysis revealed the highest As level. The raw

sienna from Tuscany (PK40400) has a high Nb content, as identified by XRF, while the IR pattern showed that this pigment and the Amberg yellow were both characterized by the presence of calcite. On the other hand, the FTIR spectrum of yellow ocher from Island (PK11551) is characterized by unidentified amorphous silicates.

4.1.3. Green Earths

The green earth samples from Cyprus can be clearly differentiated from the other green pigments by the characteristic bands ascribed to celadonite, correlated with the highest K level identified by XRF, as compared to the other green samples. XRF also revealed higher potassium for the Bavarian (PK11100) and Russian green earth (PK11110) samples. The Bavarian green earth (PK11100) stands out due to high Ga, K, Rb and Si content. According to the manufacturer, this pigment is celadonite, a green-colored soft sandstone originating from the surface of a glacial valley in South Bavaria. However, the FTIR spectrum registered on this pigment more resembles the spectrum registered on the Russian green earth, containing glauconite, than with the FTIR spectra of the Cyprus green earths. As indicated in previous studies, the sharpness of the celadonite bands can be correlated with a highly ordered structure, meaning a low extent of substitution of Al for Si in the tetrahedral layer [71]. With this in mind, the variations observed in the 3610–3350 cm^{-1} region, along with the broadening of the main absorption (987 cm^{-1}) in sample PK11100, indicate a higher Al tetrahedral substitution, meaning relative disorder within the layers compared to the other celadonite-based pigments. Compared to the Cyprus green earths, the one from Bavaria also contains quartz, a criterion that could be used to differentiate between the two sources.

The FTIR spectrum of the green earth coming from a deposit in Monte Baldo, near Verona (an important celadonite deposit known since antiquity), is characterized by a broad and undifferentiated absorption band in the hydroxyl region, which can be linked to the occupancy of the octahedral sites by various trivalent cations [85], such as Au, Al or Cr, which are present in this sample. Similar to Bavarian green earth, the Si-O stretching vibrations typically seen at 1100 and 1070 cm^{-1} are not resolved, giving rise to only one strong band shifted toward higher wavenumbers. According to previous studies [73], Kremer catalog number 11010 (Veronese green earth) was found to be an iron-rich smectite with some minor admixture of micas. These variable compositional features are most probably related to the intra-source variation of the host and/or parent rock.

The green earth pigment from Iceland (PK11552) is characterized by the highest Cr level of all the green samples, as well as by high levels of Nb, Sr, Y and Si. The infrared analysis of this sample revealed a rich quartz content, possibly accompanied by rhodizite, a rare potassium cesium–beryllium–aluminum–borate mineral, first described from complex granitic pegmatites in Central Urals, Russia [74]. However, this hypothesis is not sustained by either Raman or XRF analysis (the presence of Cs and/or Be could not be highlighted).

4.1.4. Brown and Black Earths

The FTIR spectra of the brown and black earth pigments investigated highlighted a relatively higher variation, with most of the samples having a unique spectral profile. The black earth from Andalusia (PK11280) is characterized by the presence of higher traces of Rb and Zr, as well as traces of Pb, similar to most of the other Spanish pigments, while the IR analysis showed calcite and high concentrations of iron oxides compared to the other brown and black earth pigments analyzed. Compared to the red-brown pigment from the same region (PK11276), the black earth from Andalusia contains chlorites and lower amounts of calcite and iron oxides. The gray earth from Burgundy has a rich calcite matrix (highest among the investigated brown and black earth pigments) and no kaolinite compared to the red and yellow ochers from France. The calcium content in this sample is so high that, unlike most of the other samples, in which Fe is the dominant element, for this sample, Ca is the main element, and Fe is present only in small traces, as indicated by the XRF analysis.

The FTIR spectra of raw and burnt umber from Cyprus (PK41710 and PK40610) are relatively similar, and a key feature that can be used to differentiate between the two is

the absence of goethite in the burnt umber pigment [13]. From the point of view of their elemental composition, these two pigments have the highest Cu level of all the brown pigments, as well as higher Sr. Samples PK40610 and PK40710 are the only ones in the entire set, along with yellow PK40280, containing vanadium, which overlaps the titanium Kβ peak at ~4.93 keV. These Cyprus-sourced brown pigments have a very high manganese content, as compared to the other pigments, but very low content in comparison to the brown pigment from Morocco (PK40623). As indicated by Raman analysis, this Caledonian brown pigment is a wad [4], a manganese ocher rich in hausmannite ($Mn^{2+}Mn^{3+}{}_2O_4$). The brown earth from Otranto (Italy, PK11620) has the highest chromium input in the XRF spectra, along with higher Ga, Nb, Zr and Pb, and it can be clearly differentiated in the infrared spectra from the others due to the presence of boehmite. The Van Dyck Brown (PK41050) is the only brown pigment analyzed that falls in the groups of humic earths—FITR spectra extremely characteristic within the fingerprint region.

4.2. Discrimination of Earth Pigments of Similar Hue via PCA Analysis

Principal component analysis was performed separately on the FTIR and XRF spectra registered. A multivariate analysis was applied in order to investigate to what extent this approach can discriminate between samples of similar hue but different geological origin. In both cases, PCA was performed independently on each group of pigments. For the red ochers, the IR region between 540–380 cm^{-1}, representative of absorption bands due to hematite, was tested. The IR regions 3155–3150 cm^{-1} and 920–780 cm^{-1}, used to perform PCA in yellow ochers, were selected based on the characteristic absorptions for goethite (hydroxyl stretches and bends). For the green earth pigments, IR regions (3605–3530 cm^{-1} and 1100–940 cm^{-1}) characterized by specific absorptions due to celadonites/glauconites were used, while in the case of the brown and black earth pigments, the fingerprint region (1800–380 cm^{-1}) was selected due its unique absorption pattern. Regarding XRF postprocessing, the PCA matrix was constructed using the net count rates for all elements listed in Table 3. The results of the PCA in terms of explained and cumulative variance for each model group can be seen in Table 4, separately for the FTIR and XRF data.

Table 4. PCA results.

Group of Pigments	PC	Variance Account (%)		Variance Accumulated (%)	
		PCA FTIR	PCA XRF	PCA FTIR	PCA XRF
Red ochers	PC1	96.2	97.17	96.2	97.17
	PC2	3.4	2.04	99.6	99.21
	PC3	0.3	0.65	99.9	99.86
Yellow ochers	PC1	78.9	98.45	78.9	98.45
	PC2	15.4	1.42	94.3	99.87
	PC3	3.8	0.11	98.1	99.98
	PC4	0.8	—	98.9	—
	PC5	0.3	—	99.2	—
Green earths	PC1	91.4	98.45	91.4	98.45
	PC2	7.2	1.39	98.6	99.84
	PC3	0.8	0.12	99.4	99.96
	PC4	0.4	—	99.8	—
Brown and black earths	PC1	90.1	64.51	90.1	64.51
	PC2	9.2	33.93	99.3	98.46
	PC3	0.4	1.52	99.7	99.98

Figures 7–8 show the 2D plots of the analyzed pigments in the space defined by the first two PCs for the FTIR data and within the space defined by the first three PCs for the XRF data, respectively. In most cases, the first PC is clearly the most relevant, as it explains over 90% of the total variance contained in the data. For the FTIR data, the exception is the yellow ocher group, where PC1 explains only approx. 80% of the variance. The first two PCs account for most of the variability in the case of red ochers (99.6% cumulative

variability), as well as in the case of the brown and black earth pigments (99.3% of cumulative variability).

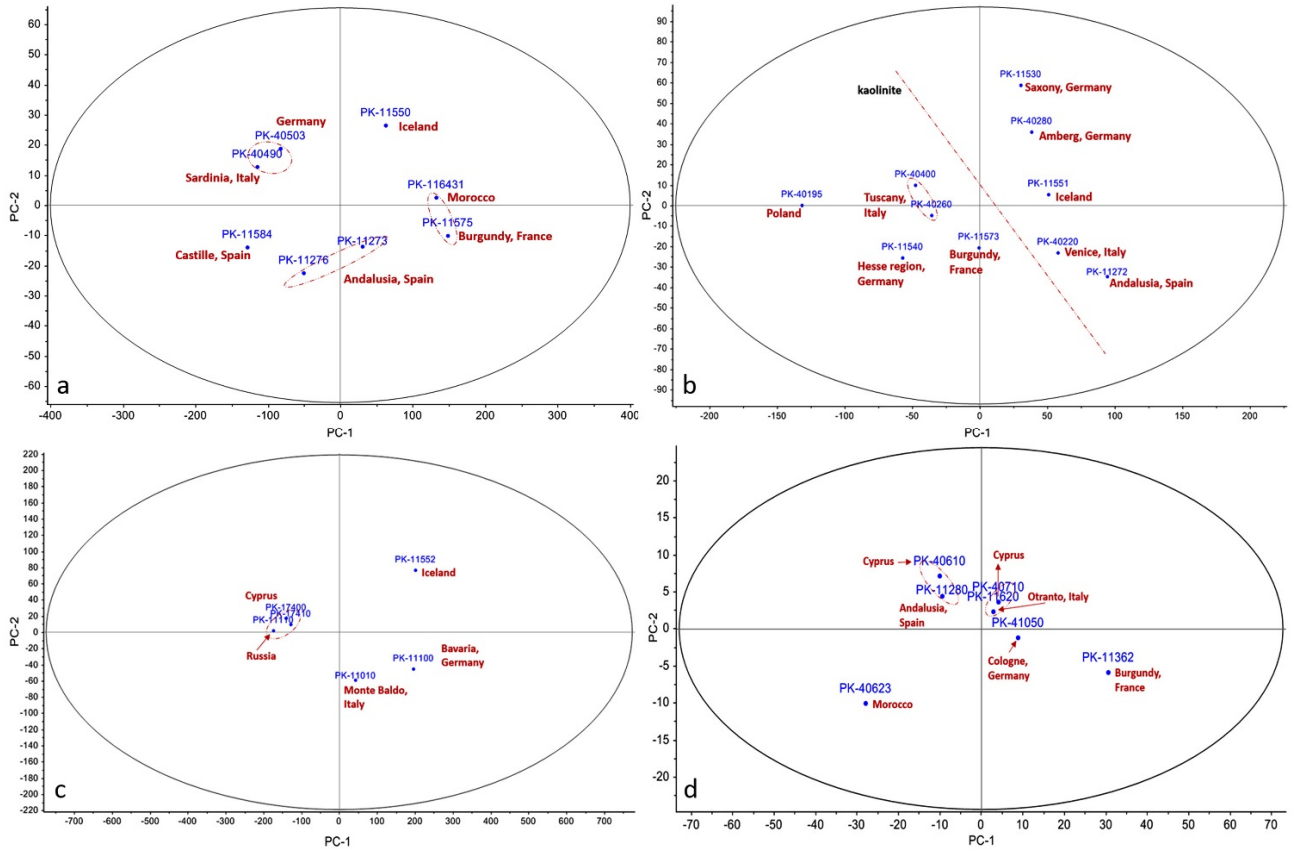

Figure 7. FTIR-PCA model of: (**a**) red ochers, (**b**) yellow ochers, (**c**) green earths, (**d**) brown and black earths.

Regarding the XRF dataset, the first PC is responsible for more than 97% of the variability in the dataset for the red, yellow and green pigments, while for the brown–black group, it only accounts for 64%, and this is probably due to the fact that pigment PK40623 acts as an outlier—it is extremely rich in manganese, which is unusual in comparison to the other pigments.

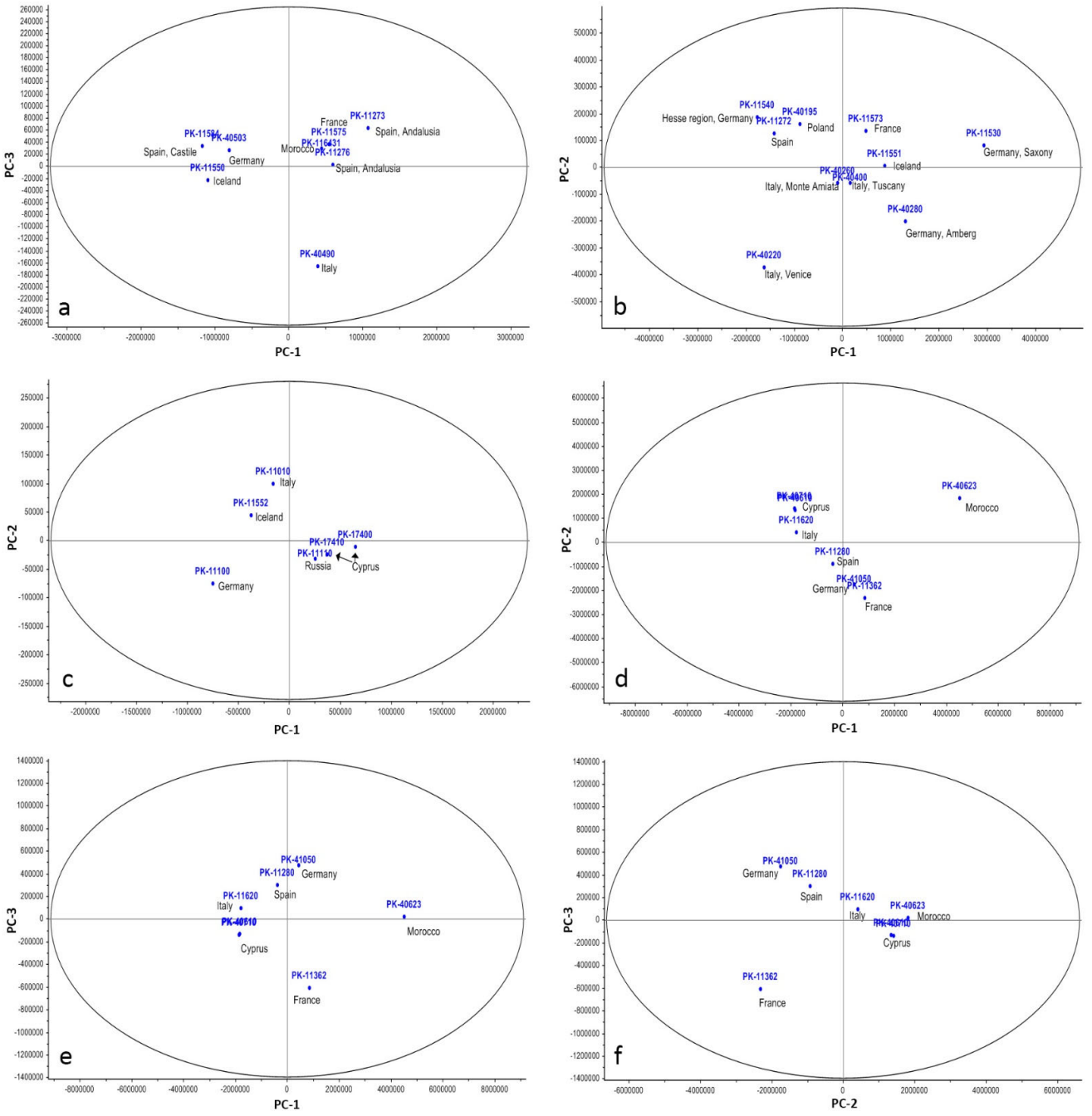

Figure 8. XRF-PCA model of: (**a**) red ochers, (**b**) yellow ochers, (**c**) green earths, (**d–f**) brown and black earths.

In the FTIR-PCA model of the red ocher samples (Figure 7a), a clear separation of the various red pigments can be observed. The score plot shows the most positive values on PC1 for the red ocher coming from Burgundy, followed by the red Moroccan ocher. The most negative values for PC1 are provided by the red ochers from Sardinia and Castile. The red earths from Iceland and Germany scored highest for PC2, while the most negative score was registered for the red ochers from Andalusia. The distribution of the samples indicates that PCA was able to detect small spectral variations within the 540–380 cm^{-1} region and discriminate among the red earth pigments based upon these. As already mentioned, the band positions (and shape) of hematite can be affected by several factors, such

as differences in crystallinity, particle size and the presence of components with overlapping absorptions. The spectral variability explained by PC1 (96.2% of the total variance) is mainly related to the absorptions of hematite, while the spectral variability explained by PC2 (3.4%) can be related to absorptions associated with other mineral components. In the XRF dataset, some similar results were obtained for the red ochers (Figure 8a). The Moroccan and French pigments appear closely related and are close to the two Andalusian pigments, while the German, Icelandic and Castille pigments show common features.

The FTIR-PCA model obtained for the yellow ochers (Figure 7b) highlights a clear separation between the yellow ochers rich in kaolinite and the other yellow ochers via the first PC, which explains 78.9% of the total variance within the dataset. All yellow ochers containing kaolinite show negative values for PC1, with the yellow ocher from Poland having the highest negative value. The yellow ochers from Saxony, Amberg and Iceland scored highest for PC2, while the one from Andalusia registered the most negative score. The two ochers from Tuscany are clustered together, indicating a close similarity. As in the case of red earths, the small spectral variations detected via PCA enabled the discrimination of the pigments. The behavior of the yellow ochers allowed a separation in accordance with their composition and general FTIR pattern. Though not apparent upon first sight, the XRF-PCA model identified lots of variability in the elemental composition of the yellow ocher pigments (Figure 8b). The pigments from the Hesse region, Germany, Poland, Tuscany and Monte Amiata are similar, in accordance with FTIR data, but some other pigments are also alongside them. The two German pigments and the Italian pigments are far from the rest. The loadings plots indicated that the PC1 is most influenced by Fe, hence the positioning of yellow pigments from Germany (PK11530 and PK11540) on the high end of PC1 scale, while PC2's variability is provided by Ca, Sr, S, Si, Rb, K and Zr, which explains the presence of PK11540, PK40195, PK11272 and PK40220 on the extremities of the PC2 scale. PK11540 and PK40195, from Germany and Poland, respectively, are high in K, Rb, Si and Zr; PK11272 (from Spain) shows the highest Si input, and PK40220 (from Venice, Italy) has the highest S and Sr content, as well as high Ca.

The score plot of the PCA performed on the spectra of green earths highlights a clustering of the samples from Cyprus and Russia (highest negative score on PC1) for both the FTIR (Figure 7c) and the XRF data (Figure 8c). FTIR data indicated a clear separation in the sample from Iceland (highest positive score on both PC1 and PC2), but this was not the case for the XRF dataset, which placed this pigment near the one from Italy (PK11010). The celadonites from Verona and Bavaria are characterized by the highest negative scores on the PC2. The first PC explains over 91% of the total variance in both datasets, and with the exception of the Russian green earth (containing glauconite), all other samples are clearly separated. As shown in previous studies [4,7], glauconite and celadonite have very similar chemistries and are extremely difficult to distinguish using most available analytical techniques. The two minerals differ, however, in terms of origin, as they have very different environments of formation (celadonite occurs through the alteration of basaltic igneous rocks, while glauconite is derived from marine clays and sandstones/greensands), and this knowledge (if available) can be used to determine the provenance of green earth pigments.

In the FTIR-PCA model of the brown and black pigments (Figure 7d), some clusters can be observed. The black earth from Andalusia and the raw umber from Cyprus scored highest on PC2 and are relatively well grouped. Another cluster is represented by the burnt umber from Cyprus and the brown earth from Otranto (high positive values on PC2 and intermediate values on PC1). The gray earth from Burgundy scored highest on PC1, followed by Cologne brown, while the most negative score for PC1 was obtained by the brown earth from Morocco.

Compared to the other FTIR-PCA models, the one on brown and black pigments shows a lower capability to discriminate pigments based on their IR spectral signatures in the fingerprint region. Regarding the XRF dataset (Figure 8d), the brown pigment from Morocco (PK40623) is clearly delimited from the rest, which is understandable given the fact that PC1 is highly influenced by Mn and Pb, and this pigment has the highest manganese content of all samples. Similar to the green ones, the brown pigments from Cyprus

are grouped together, indicating very similar features, as also indicated by the FTIR data. Although French gray pigment PK11362 was expected to be separated from the rest, as it has an inverse Ca:Fe ratio compared to the rest of the pigments, it appears only slightly differentiated in the score plot of the first two PCs. However, a much clearer separation is observed when plotting PC1 or PC2 versus the third principal component (Figure 8e,f), due to the fact that Fe has the highest (negative) value on the PC3 scale.

Based on the overall results, the application of PCA on the FTIR and XRF data marked some advantages when compared to direct spectral analysis, and it demonstrated a good ability to discriminate between the various investigated samples. By applying PCA to narrow IR regions (characteristic of the absorptions of the various chromophore phases associated with the investigated earth pigments), in most of the cases, a relatively clear separation was obtained, highlighting a promising tool for the classification of earth pigments of similar color but different provenance.

5. Conclusions

The objective of this study was to determine if it is possible to discriminate between earth pigments of similar color tones from different locations using spectral and chemical fingerprints derived from easily accessible spectroscopic techniques. Molecular, structural and chemical characterization were carried out via FTIR, Raman and XRF spectroscopy on 31 natural earth pigments from various geographical locations, and multivariate analysis was performed to further explore both FTIR and XRF datasets.

FTIR analysis provided important information on the characteristics of the coloring agent (such as particle size and shape and degree of crystallinity) as well as on the various accessory minerals present. For most situations, FTIR spectroscopy proved to be a powerful experimental method for studying the molecular structure of earth pigments. However, there are situations when spectral interferences (generated by overlapping absorptions) hinder a clear identification of the different minerals that may be present. As shown in this study, these types of problems can be, in general, easily overcome using Raman analysis. Nonetheless, in some of the cases, characterization by Raman spectroscopy was not possible due to fluorescence phenomena (analytical limitations caused by the fact that only one excitation wavelength was available in the experimental setup).

From the perspective of their elemental composition, as identified through XRF, the results showed a highly similar composition, with Fe being the major element in most of the cases, followed by either minor or trace inputs of Ca, Ti, K or Mn, plus a wide range of other accessory elements. With such similarity, differentiation between the selected pigments is a very difficult task; however, some trends could be evidenced, either related to the source of origin or to the color of the pigment. The detection of low-Z elements, such as Na and Mg, was not achieved above the detection limit for any of the investigated pigments, a clear limitation of airpath XRF spectrometers.

Attempts to distinguish earth pigments of similar color from different locations based only on their FTIR spectra showed several limitations, especially for samples that have extremely similar IR signatures. Although the presence of accessory minerals can limit the identification of chromophore phases (iron oxides/hydroxides, celadonites, etc.), in some situations, their presence can be linked to a particular geological source, allowing pigments of similar hue to be distinguished. Principal component analysis performed on FTIR datasets improved sample classification and highlighted that the small spectral variations observed in the IR regions, where the chromophore species give rise to characteristic absorptions, can be detected and used to classify and discriminate between pigments according to their origin.

The study demonstrates the value of using easily accessible complementary spectroscopic techniques as a preliminary step for the qualitative characterization and differentiation of earth pigments and how chemometric analysis can inform and enhance the interpretation of spectral and chemical trends. The obtained results contribute to the knowledge and understanding of the complex chemistry of earth pigments, including of pigments never studied before, such as the ones originating from Iceland. Moreover, the multivariate discrimination

models proposed showed promising results, highlighting a potential tool that could be used for provenance research, if further refined. Good discrimination was achieved for Andalusian pigments, which could be differentiated even from other Spanish-sourced pigments. Another good differentiation was obtained for pigments coming from Cyprus, both the brown and the green ones. Furthermore, French and Moroccan pigments are separated from the rest, while pigments from Germany or Italy sometimes have overlapping features.

Finally, registered spectra can be used as reference datasets to speed up the identification of unknown pigments, but a series of aspects need to be taken into account when other users compare their spectra with those of our study, such as: changes in composition due to processing (depending on the manufacturer), variation in pigment geochemistry within the source (intra-source variation) or the possible geological similarity of ochers from different locations.

Supplementary Materials: The following supporting information can be downloaded at: https://www.mdpi.com/article/10.3390/min12060755/s1. Figure S1. Elemental distribution for all analyzed pigments. Figure S2. Raw XRF data (full data set). Figure S3. Raw Raman data (785 nm). Figure S4. Loading plots (FTIR-PCA).

Author Contributions: Conceptualization, I.M.C.; methodology, I.M.C., L.G. and R.R.; investigation and data curation, I.M.C. and L.G.; formal analysis: I.M.C., L.G., R.R. and G.S.; writing—original draft preparation, I.M.C., L.G., R.R. and G.S.; writing—review and editing, I.M.C. and L.G.; funding acquisition, I.M.C. All authors have read and agreed to the published version of the manuscript.

Funding: This research was funded by a grant of the Romanian Ministry of Education and Research, UEFISCDI (The Executive Unit for the Financing of Higher Education, Research, Development and Innovation), project number PN-III-P1-1.1-PD-2019-1099, within PNCDI III.

Data Availability Statement: The data that support the findings of this study are available upon request from the corresponding authors.

Conflicts of Interest: The authors declare that they have no competing interests.

References

1. Domingo, I.; Chieli, A. Characterizing the pigments and paints of prehistoric artists. *Archaeol Anthropol Sci*. **2021**, *13*, 166. https://doi.org/10.1007/s12520-021-01397-y.
2. Berrie, B.H. *Artists' Pigments: A Handbook of Their History and Characteristics*; Archetype Publications: London, UK, 2007; Volume 4.
3. Henshilwood, C.S.; d'Errico, F.; Watts, I. Engraved ochres from the Middle Stone Age levels at Blombos Cave, South Africa. *J. Hum. Evol.* **2009**, *57*, 27–47. https://doi.org/10.1016/j.jhevol.2009.01.005.
4. Siddall, R. Mineral pigments in archaeology: Their analysis and the range of available materials. *Minerals* **2018**, *8*, 201. https://doi.org/10.3390/min8050201.
5. Barham, L.S. Systematic pigment use in the middle pleistocene of south-central Africa. *Curr. Anthropol.* **2002**, *43*, 181–190. https://doi.org/10.1086/338292.
6. d'Errico, F.; Dayet Bouillot, L.; García-Diez, M.; Pitarch Martí, A.; Garrido Pimentel, D.; Zilhão, J. The technology of the earliest European cave paintings: El Castillo Cave, Spain. *J. Archaeol. Sci.* **2016**, *70*, 48–65. https://doi.org/10.1016/j.jas.2016.03.007.
7. Eastaugh, N.; Walsh, V.; Chaplin, T.; Siddall, R. *Pigment Compendium: A Dictionary and Optical Microscopy of Historical Pigments*, 1st ed.; Routledge: London, UK, 2008. https://doi.org/10.4324/9780080943596.
8. Bikiaris, D.; Daniilia, S.; Sotiropoulou, S.; Katsimbiri, O.; Pavlidou, E.; Moutsatsou, A.P.; Chryssoulakis, Y. Ochre-differentiation through micro-Raman and micro-FTIR spectroscopies: Application on wall paintings at Meteora and Mount Athos, Greece. *Spectrochim. Acta A* **2000**, *56*, 3–18. https://doi.org/10.1016/S1386-1425(99)00134-1.
9. Popelka-Filcoff, R.S.; Robertson, J.D.; Glascock, M.D.; Descantes, C. Trace element characterization of ochre from geological sources. *J. Radioanal. Nucl. Chem.* **2007**, *272*, 17–27. https://doi.org/10.1007/s10967-006-6836-x.
10. Helwig, K. The characterisation of iron earth pigments using infrared spectroscopy. In Proceedings of the Second Infrared and Raman User's Group (IRUG 2) Conference, Victoria and Albert Museum, London, UK, 12–13 September 1995; pp. 83–92.
11. Huntley, J. Australian Indigenous Ochres: Use, Sourcing, and Exchange. In *The Oxford Handbook of the Archaeology of Indigenous Australia and New Guinea*; McNiven, I.J., David, B., Eds.; Oxford University Press: New York, NY, USA, 2021. https://doi.org/10.1093/oxfordhb/9780190095611.013.21.
12. Elias, M.; Chartier, C.; Prévot, G.; Garay, H.; Vignaud, C. The colour of ochres explained by their composition. *Mater. Sci. Eng. B Solid-State Mater. Adv. Technol.* **2006**, *127*, 70–80. https://doi.org/10.1016/j.mseb.2005.09.061.
13. Genestar, C.; Pons, C. Earth pigments in painting: Characterisation and differentiation by means of FTIR spectroscopy and SEM-EDS microanalysis. *Anal. Bioanal. Chem.* **2005**, *382*, 269–274. https://doi.org/10.1007/s00216-005-3085-8.

14. Kostomitsopoulou Marketou, A.; Kouzeli, K.; Facorellis, Y. Colourful earth: Iron-containing pigments from the Hellenistic pigment production site of the ancient agora of Kos (Greece). *J. Archaeol. Sci. Rep.* **2019**, *26*, 101843. https://doi.org/10.1016/j.jasrep.2019.05.008.
15. Marshall, L.J.R.; Williams, J.R.; Almond, M.J.; Atkinson, S.D.M.; Cook, S.R.; Matthews, W.; Mortimore, J.L. Analysis of ochres from Clearwell Caves: The role of particle size in determining colour. *Spectrochim. Acta A* **2005**, *61*, 233–241. https://doi.org/10.1016/j.saa.2004.03.041.
16. Rousaki, A.; Vargas, E.; Vázquez, C.; Aldazábal, V.; Bellelli, C.; Carballido Calatayud, M.; Hajduk, A.; Palacios, O.; Moens, L.; Vandenabeele, P. On-field Raman spectroscopy of Patagonian prehistoric rock art: Pigments, alteration products and substrata. *Trends Analyt Chem.* **2018**, *105*, 338–351. https://doi.org/10.1016/j.trac.2018.05.011.
17. Boucherie, N.; Nowik, W.; Pingaud, N. Characterisation of materials and techniques in first archaeological findings of Nasca wall paintings. *Herit. Sci.* **2021**, *9*, 63. https://doi.org/10.1186/s40494-021-00535-y.
18. Cortea, I.M.; Ratoiu, L.; Ghervase, L.; Țentea, O.; Dinu, M. Investigation of ancient wall painting fragments discovered in the roman baths from alburnus maior by complementary non-destructive techniques. *Appl. Sci.* **2021**, *11*, 10049. https://doi.org/10.3390/app112110049.
19. Bianchin, S.; Casellato, U.; Favaro, M.; Vigato, P.A. Painting technique and state of conservation of wall paintings at Qusayr Amra, Amman–Jordan. *J. Cult. Herit.* **2007**, *8*, 289-293. https://doi.org/10.1016/j.culher.2007.05.002.
20. Edreira, M.C.; Feliu, M.J.; Fernández-Lorenzo, C.; Martín, J. Spectroscopic analysis of Roman wall paintings from Casa del Mitreo in Emerita Augusta, Mérida, Spain. *Talanta* **2003**, *59*, 1117–1139. https://doi.org/10.1016/S0039-9140(03)00020-1.
21. Mastrotheodoros, G.P.; Beltsios, K.G.; Bassiakos, Y. On the Red and Yellow Pigments of Post-Byzantine Greek Icons. *Archaeometry* **2020**, *63*, 753–778. https://doi.org/10.1111/arcm.12642.
22. Ghervase, L.; Cortea, I.M.; Rădvan, R.; Ratoiu, L.; Chelmuș, A. Complementary investigations of two Lipovan-style icons. *Microchem. J.* **2018**, *138*, 509–518. https://doi.org/10.1016/j.microc.2018.01.047.
23. Antunes, V.; Candeias, A.; Mirão, J.; Carvalho, M.L.; Dias, C.B.; Manhita, A.; Cardoso, A.; Francisco, M.J.; Lauw, A.; Manso, M. Analytical characterization of the palette and painting techniques of Jorge Afonso, the great 16th century Master of Lisbon painting workshop. *Spectrochim. Acta A* **2018**, *193*, 264–275. https://doi.org/10.1016/j.saa.2017.12.027.
24. Cortea, I.M.; Ghervase, L.; Ratoiu, L.; Dinu, M.; Rădvan, R. Uncovering hidden jewels: An investigation of the pictorial layers of an 18th-century Taskin harpsichord. *Herit. Sci.* **2020**, *8*, 55. https://doi.org/10.1186/s40494-020-00401-3.
25. van Loon, A.; Vandivere, A.; Delaney, J.K.; Dooley, K.A.; De Meyer, S.; Vanmeert, F.; Gonzalez, V.; Janssens, K.; Leonhardt, E.; Haswell, R.; et al. Beauty is skin deep: The skin tones of Vermeer's Girl with a Pearl Earring. *Herit. Sci.* **2019**, *7*, 102. https://doi.org/10.1186/s40494-019-0344-0.
26. Grygar, T.; Hradilová, J.; Hradil, D.; Bezdička, P.; Bakardjieva, S. Analysis of earthy pigments in grounds of Baroque paintings. *Anal. Bioanal. Chem.* **2003**, *375*, 1154–1160. https://doi.org/10.1007/s00216-002-1708-x.
27. Popelka-Filcoff, R.S.; Miksa, E.J.; Robertson, J.D.; Glascock, M.D.; Wallace, H. Elemental analysis and characterization of ochre sources from Southern Arizona. *J. Archaeol. Sci.* **2008**, *35*, 752–762. https://doi.org/10.1016/j.jas.2007.05.018.
28. MacDonald, B.L.; Fox, W.; Dubreuil, L.; Beddard, J.; Pidruczny, A. Iron oxide geochemistry in the Great Lakes Region (North America): Implications for ochre provenance studies. *J. Archaeol. Sci. Rep.* **2018**, *19*, 476–490. https://doi.org/10.1016/j.jasrep.2018.02.040.
29. MacDonald, B.L.; Hancock, R.G.V.; Cannon, A.; Pidruczny, A. Geochemical characterization of ochre from central coastal British Columbia, Canada. *J. Archaeol. Sci.* **2011**, *38*, 3620–2630. https://doi.org/10.1016/j.jas.2011.08.032.
30. Gil, M.; Carvalho, M.L.; Seruya, A.; Candeias, A.E.; Mirão, J.; Queralt, I. Yellow and red ochre pigments from southern Portugal: Elemental composition and characterization by WDXRF and XRD. *Nucl. Instrum. Methods Phys. Res. A Accel. Spectrom. Detect. Assoc. Equip.* **2007**, *580*, 728–731. https://doi.org/10.1016/j.nima.2007.05.131.
31. Hradil, D.; Píšková, A.; Hradilová, J.; Bezdička, P.; Lehrberger, G.; Gerzer, S. Mineralogy of bohemian green earth pigment and its microanalytical evidence in historical paintings. *Archaeometry* **2011**, *53*, 563–586. https://doi.org/10.1111/j.1475-4754.2010.00554.x.
32. Weinstein-Evron, M.; Ilani, S. Provenance of ochre in the natufian layers of el-Wad Cave, Mount Carmel, Israel. *J. Archaeol. Sci.* **1994**, *21*, 461–467. https://doi.org/10.1006/jasc.1994.1045.
33. Erlandson, J.M.; Robertson, J.D.; Descantes, C. Geochemical Analysis of Eight Red Ochres from Western North America. *Am. Antiq.* **1999**, *64*, 517–526. https://doi.org/10.2307/2694149.
34. Dayet, L.; Le Bourdonnec, F.X.; Daniel, F.; Porraz, G.; Texier, P.J. Ochre Provenance and Procurement Strategies During The Middle Stone Age at Diepkloof Rock Shelter, South Africa. *Archaeometry* **2016**, *58*, 807–829. https://doi.org/10.1111/arcm.12202.
35. Popelka-Filcoff, R.S.; Zipkin, A.M. The archaeometry of ochre sensu lato: A review. *J. Archaeol. Sci.* **2022**, *137*, 105530. https://doi.org/10.1016/j.jas.2021.105530.
36. Dayet, L. Invasive and non-invasive analyses of ochre and iron-based pigment raw materials: A methodological perspective. *Minerals* **2021**, *11*, 210. https://doi.org/10.3390/min11020210.
37. Genestar, C.J.; Pons Bonafé, C. The use of natural earths in picture: Study and differentiation by thermal analysis. *Thermochim. Acta* **2004**, *413*, 185–192. https://doi.org/10.1016/j.tca.2003.10.016.
38. Nel, P.; Lynch, P.A.; Laird, J.S.; Casey, H.M.; Goodall, L.J.; Ryan, C.G.; Sloggett, R.J. Elemental and mineralogical study of earth-based pigments using particle induced X-ray emission and X-ray diffraction. *Nucl. Instrum. Methods Phys. Res. A Accel. Spectrom. Detect. Assoc. Equip.* **2010**, *619*, 306–310. https://doi.org/10.1016/j.nima.2009.12.003.

39. Fanost, A.; Gimat, A.; de Viguerie, L.; Martinetto, P.; Giot, A.C.; Clémancey, M.; Blondin, G.; Gaslain, F.; Glanville, H.; Walter, P.; et al. Revisiting the identification of commercial and historical green earth pigments. *Colloids Surf. A Physicochem. Eng. Asp.* **2020**, *584*, 124035. https://doi.org/10.1016/j.colsurfa.2019.124035.
40. Doménech, A.; Doménech-Carbó, M.T.; Edwards, H.G.M. Identification of earth pigments by applying hierarchical cluster analysis to solid state voltammetry. Application to severely damaged frescoes. *Electroanalysis* **2007**, *19*, 1890–1900. https://doi.org/10.1002/elan.200703948.
41. de Faria, D.L.A.; Lopes, F.N. Heated goethite and natural hematite: Can Raman spectroscopy be used to differentiate them? *Vib. Spectrosc.* **2007**, *45*, 117–121. https://doi.org/10.1016/j.vibspec.2007.07.003.
42. Froment, F.; Tournié, A.; Colomban, P. Raman identification of natural red to yellow pigments: Ochre and iron-containing ores. *J. Raman Spectrosc.* **2008**, *39*, 560–568. https://doi.org/10.1002/jrs.1858.
43. Ospitali, F.; Bersani, D.; Di Lonardo, G.; Lottici, P.P. 'Green earths': Vibrational and elemental characterization of glauconites, celadonites and historical pigments. *J. Raman Spectrosc.* **2008**, *39*, 1066–1073. https://doi.org/10.1002/jrs.1983.
44. David, B.; Clayton, E.; Watchman, A. Initial Results Of Pixe Analysis On Northern Australian Ochres. *Aust. Archaeol.* **1993**, *36*, 50–57. https://doi.org/10.1080/03122417.1993.11681482.
45. Makreski, P.; Jovanovski, G.; Kaitner, B. Minerals from Macedonia. XXIV. Spectra-structure characterization of tectosilicates. *J. Mol. Struct.* **2009**, *924*, 413–419. https://doi.org/10.1016/j.molstruc.2009.01.001.
46. Béarat, H. Les Pigments Verts En Peinture Murale Romaine: Bilan Analytique. In Roman Wall Painting: Materials, Techniques, Analysis and Conservation In Proceedings of the International Workshop on Roman Wall Painintg, Fribourg, Switzerland, 7–9 March 1996; pp. 269–286.
47. Cavallo, G.; Riccardi, M.P.; Zorzin, R. Powder diffraction of yellow and red natural earths from Lessini Mountains in NE Italy. *Powder Diffr.* **2015**, *30*, 122–129. https://doi.org/10.1017/S0885715614001407.
48. Farmer, V.C. *The Infrared Spectra of Minerals*; Mineralogical Society: London, UK, 1974. https://doi.org/10.1180/mono-4.
49. Mcmillan, P.F.; Hofmeister, A.M. Infrared and Raman spectroscopy. In *Spectroscopic Methods in Mineralogy and Geology;* Hawthorne, F.C., Ed.; Mineralogical Society of America: Washington, DC, USA, 1988; Volume 18, pp. 99–160. https://doi.org/10.1515/9781501508974-006.
50. Shugar, A.N.; Mass, J.L. *Handheld XRF for Art and Archaeology*; Leuven University Press: Leuven, Belgium, 2013.
51. Pozzi, F.; Rizzo, A.; Basso, E.; Angelin, E.M.; Sá, S.F.; Cucci, C.; Picollo, M. Portable Spectroscopy for Cultural Heritage. In *Portable Spectroscopy and Spectrometry II—Applications*, 1st ed.; Crocombe, R.A., Leary, P.E., Kammrath, B.W., Eds.; Wiley: Hoboken, NJ, USA, 2021; pp. 499–522. https://doi.org/10.1002/9781119636489.ch43.
52. Wei, C.; Wang, J.; Ji, J. Forensic Classification of Pigments by Attenuated Total Reflectance–Fourier Transform Infrared Spectroscopy and Chemometrics. *Anal. Lett.* **2021**, *54*, 1309–1328. https://doi.org/10.1080/00032719.2020.1801712.
53. Festa, G.; Scatigno, C.; Armetta, F.; Saladino, M.L.; Ciaramitaro, V.; Nardo, V.M.; Ponterio, R.C. Chemometric Tools to Point Out Benchmarks and Chromophores in Pigments through Spectroscopic Data Analyses. *Molecules* **2022**, *27*, 163. https://doi.org/10.3390/molecules27010163.
54. Mauran, G.; Caron, B.; Détroit, F.; Nankela, A.; Bahain, J.J.; Pleurdeau, D.; Lebon, M. Data pretreatment and multivariate analyses for ochre sourcing: Application to Leopard Cave (Erongo, Namibia). *J. Archaeol. Sci. Rep.* **2021**, *35*, 102757. https://doi.org/10.1016/j.jasrep.2020.102757.
55. Esbensen, K.H.; Geladi, P. Principal Component Analysis: Concept, Geometrical Interpretation, Mathematical Background, Algorithms, History, Practice. In *Comprehensive Chemometrics*, 1st ed.; Brown, S.D., Tauler, R., Walczak, B., Eds.; Elsevier: Amsterdam, The Netherlands, 2009; Volume 1, pp. 211–226. https://doi.org/10.1016/B978-044452701-1.00043-0.
56. Peris-Díaz, M.D.; Krężel, A. A guide to good practice in chemometric methods for vibrational spectroscopy, electrochemistry, and hyphenated mass spectrometry. *Trends Analyt Chem.* **2021**, *135*, 116157. https://doi.org/10.1016/j.trac.2020.116157.
57. Aida, S.; Matsuno, T.; Hasegawa, T.; Tsuji, K. Application of principal component analysis for improvement of X-ray fluorescence images obtained by polycapillary-based micro-XRF technique. *Nucl. Instrum. Meth. B* **2017**, *402*, 267–273. https://doi.org/10.1016/j.nimb.2017.03.123.
58. Invernizzi, C.; Fiocco, G.; Iwanica, M.; Targowski, P.; Piccirillo, A.; Vagnini, M.; Licchelli, M.; Malagodi, M.; Bersani, D. Surface and interface treatments on wooden artefacts: Potentialities and limits of a non-invasive multi-technique study. *Coatings* **2021**, *11*, 29. https://doi.org/10.3390/coatings11010029.
59. Andrić, V.; Gajić-Kvaščev, M.; Korolija Crkvenjakov, D.; Marić-Stojanović, M.; Gadžurić, S. Evaluation of pattern recognition techniques for the attribution of cultural heritage objects based on the qualitative XRF data. *Microchem. J.* **2021**, *167*, 106267. https://doi.org/10.1016/j.microc.2021.106267.
60. Salama, W.; El Aref, M.; Gaupp, R. Spectroscopic characterization of iron ores formed in different geological environments using FTIR, XPS, Mössbauer spectroscopy and thermoanalyses. *Spectrochim. Acta A* **2015**, *136*, 1816–1826. https://doi.org/10.1016/j.saa.2014.10.090.
61. Saikia, B.J.; Parthasarathy, G.; Sarmah, N.C.; Fourier transform infrared spectroscopic estimation of crystallinity in SiO2 based rocks. *Bull. Mater. Sci.* **2008**, *31*, 775–779. https://doi.org/10.1007/s12034-008-0123-0.
62. Miliani, C.; Rosi, F.; Daveri, A.; Brunetti, B.G. Reflection infrared spectroscopy for the non-invasive in situ study of artists' pigments. *Appl. Phys. A Mater. Sci. Process.* **2012**, *106*, 295–307. https://doi.org/10.1007/s00339-011-6708-2.
63. Roy, A. *Artists' Pigments. A Handbook of Their History and Characteristics*; National Gallery of Art: Washington, DC, USA, 1993; Volume 2.

64. Vahur, S.; Teearu, A.; Leito, I. ATR-FT-IR spectroscopy in the region of 550-230 cm^{-1} for identification of inorganic pigments. *Spectrochim. Acta A* **2010**, *75*, 1061–1072. https://doi.org/10.1016/j.saa.2009.12.056.
65. Cambier, P. Infrared study of goethites of varying crystallinity and particle size: I. Interpretation of OH and lattice vibration frequencies. *Clay Miner.* **1986**, *21*, 191–200. https://doi.org/10.1180/claymin.1986.021.2.08.
66. Schwertmann, U.; Cambier, P.; Murad, E. Properties of goethites of varying crystallinity. *Clays Clay Miner.* **1985**, *33*, 369–378. https://doi.org/10.1346/CCMN.1985.0330501.
67. Jovanovski, G.; Makreski, P.; Kaitner, B.; Šoptrajanov, B. Minerals from Macedonia. X-ray powder diffraction vs. vibrational spectroscopy in mineral identification. *Contrib. Sect. Nat. Math. Biotech. Sci.* **2009**, *30*, 7–34. https://doi.org/10.20903/csnmbs.masa.2009.30.1-2.22.
68. Equeenuddin, S.M.; Tripathy, S.; Sahoo, P.K.; Panigrahi, M.K. Geochemistry of ochreous precipitates from coal mine drainage in India. *Environ. Earth Sci.* **2010**, *61*, 723–731. https://doi.org/10.1007/s12665-009-0386-9.
69. Bigham, J.M.; Nordstrom, D.K. Iron and aluminum hydroxysulfates from acid sulfate waters. *Rev. Mineral. Geochem.* **2000**, *40*, 351–403. https://doi.org/10.2138/rmg.2000.40.7.
70. Madejová, J.; Gates, W.P.; Petit, S. IR Spectra of Clay Minerals. In *Developments in Clay Science*; Gates, W.P., Kloprogge, J.T., Madejová, J., Bergaya, F., Eds.; Elsevier: Amsterdam, The Netherlands, 2017; Volume 8, pp. 107–149. https://doi.org/10.1016/B978-0-08-100355-8.00005-9.
71. Buckley, H.A.; Bevan, J.C.; Brown, K.M.; Johnson, L.R.; Farmer, V.C. Glauconite and celadonite: Two separate mineral species. *Mineral. Mag.* **1978**, *42*, 373–382. https://doi.org/10.1180/minmag.1978.042.323.08.
72. Feller, R.L. *Artists' Pigments: A Handbook of Their History and Characteristics*; National Gallery of Art: Washington, DC, USA, 1986; Volume 1.
73. Hradil, D.; Grygar, T.; Hrušková, M.; Bezdička, P.; Lang, K.; Schneeweiss, O.; Chvátal, M. Green earth pigment from the Kadaň region, Czech Republic: Use of rare Fe-rich smectite. *Clays Clay Miner*. **2004**, *52*, 767–778. https://doi.org/10.1346/CCMN.2004.0520612.
74. Frost, R.L.; López, A.; Xi, Y.; Scholz, R.; Souza, L.; Lana, C. The molecular structure of the borate mineral rhodizite (K, Cs)Al 4Be4(B, Be)12O28—A vibrational spectroscopic study. *Spectrochim. Acta A* **2014**, *128*, 291–294. https://doi.org/10.1016/j.saa.2014.02.036.
75. Hradil, D.; Grygar, T.; Hradilová, J.; Bezdička, P. Clay and iron oxide pigments in the history of painting. *Appl. Clay Sci.* **2003**, *22*, 223–236. https://doi.org/10.1016/S0169-1317(03)00076-0.
76. McKeown, D.A.; Post, J.E.; Etz, E.S. Vibrational analysis of palygorskite and sepiolite. *Clays Clay Miner.* **2002**, *50*, 667–680. https://doi.org/10.1346/000986002320679549.
77. Li, L.; Zhang, Y.; Zhang, Y.; Sun, J.; Wang, Z. The thermal transmission behavior analysis of two coal gangues selected from Inner Mongolia In China. *Therm. Sci.* **2018**, *22*, 1111–1119. https://doi.org/10.2298/TSCI160727272L.
78. Tomasini, E.; Siracusano, G.; Maier, M.S. Spectroscopic, morphological and chemical characterization of historic pigments based on carbon. Paths for the identification of an artistic pigment. *Microchem. J.* **2012**, *102*, 28–37. https://doi.org/10.1016/j.microc.2011.11.005.
79. Fitz Hugh, E.W. *Artists' Pigments: A Handbook of Their History and Characteristics*; National Gallery of Art: Washington, DC, USA, 1997; Volume 3.
80. Smith, B.C. *Infrared Spectral Interpretation: A Systematic Approach*, 1st ed.; CRC Press: Boca Raton, FL, USA, 1999.
81. Bernardini, S.; Bellatreccia, F.; Della Ventura, G.; Ballirano, P.; Sodo, A. Raman spectroscopy and laser-induced degradation of groutellite and ramsdellite, two cathode materials of technological interest. *RSC Adv.* **2020**, *10*, 923–929. https://doi.org/10.1039/c9ra08662e.
82. Rogerio-Candelera, M.Á.; Herrera, L.K.; Miller, A.Z.; García Sanjuán, L.; Mora Molina, C.; Wheatley, D.W.; Justo, Á.; Saiz-Jimenez, C. Allochthonous red pigments used in burial practices at the Copper Age site of Valencina de la Concepción (Sevilla, Spain): Characterisation and social dimension. *J. Archaeol. Sci.* **2013**, *40*, 279–290. https://doi.org/10.1016/j.jas.2012.08.004.
83. Bibi, I.; Icenhower, J.; Niazi, N.K.; Naz, T.; Shahid, M.; Bashir, S. Clay Minerals: Structure, Chemistry, and Significance in Contaminated Environments and Geological CO2 Sequestration. In *Environmental Materials and Waste: Resource Recovery and Pollution Prevention*, 1st ed.; Prasad, M.N.V., Shih, K., Eds.; Academic Press: London, UK, 2016; pp. 543–567. https://doi.org/10.1016/C2014-0-05144-1.
84. Kupka, D.; Pállová, Z.; Horňáková, A.; Achimovičová, M.; Kavečanský, V. Effluent water quality and the ochre deposit characteristics of the abandoned Smolník mine, East Slovakia. *Acta Montan. Slovaca* **2012**, *17*, 56–64.
85. Odin, G.S.; Desprairies, A.; Fullagar, P.D.; Bellon, H.; Decarreau, A.; Frohlich, F.; Zelvelder, M. Nature and Geological Significance of Celadonite. In *Developments in Sedimentology*; Odin, G.S., Ed.; Elsevier: Amsterdam, The Netherlands, 1988; Volume 45, pp. 337–398. https://doi.org/10.1016/S0070-4571(08)70071-2.